

A class of d -dimensional regular black holes: Shadows, Thermodynamics and Gravitational collapse

A. Sadeghi¹, F. Shojai¹

Department of Physics, University of Tehran, P.O. Box 14395-547
Tehran, Iran.

February 12, 2026

Abstract

This paper examines a recently introduced class of regular black holes that can form from the collapse of a polytropic star with an arbitrary polytropic index. This class has a de Sitter core and reduces to the Bardeen and Hayward black holes when the polytropic index is chosen appropriately. We demonstrate that this class of black holes is sourced by a nonlinear electrodynamics Lagrangian in d dimensions and that its regularity stems from the presence of magnetic charge. We analyze the energy conditions and study the photon spheres analytically and the shadows numerically. Then, we compare our results with observations. Additionally, we present the thermodynamic properties of this class of black holes, including their temperature, entropy, and heat capacity. We also examine their thermodynamic stability. Finally, we generalize the Oppenheimer-Snyder-Datt collapse scenario to this d -dimensional class of black holes and study stellar collapse into them, as well as the evolution of the star's surface, the apparent horizon, and the event horizon.

1 Introduction

The black hole (BH) singularity is associated with the divergence of curvature invariants. It is generally believed that such a singularity would not exist in a complete theory of quantum gravity [1]. According to the weak cosmic censorship conjecture, if stellar matter satisfies the null energy condition (NEC), the BH singularity remains hidden behind the event horizon, thereby preserving the predictable structure of spacetime [2]. In general relativity, BHs represent the ultimate state of classical gravitational collapse for massive stars. However, it has been proposed that quantum effects could produce a repulsive pressure that counteracts gravitational attraction and prevents the formation of a singularity at the end of collapse [1].

Several approaches have been suggested to eliminate singularities in BHs. One method involves modifying the Einstein-Hilbert action by incorporating additional terms arising from vacuum polarization and particle creation [3]. Another approach imposes an upper bound on spacetime curvature [4, 5]. Early efforts were inspired by Einstein and Rosen's concept of wormhole geometry. Later, Sakharov proposed using the equation of state $p = -\rho$ for high density regions in stars [6], while Gliner suggested that such conditions could represent the final state of gravitational collapse [7].

Here, we focus on regular BHs with de Sitter cores. Hayward and Bardeen introduced two important solutions. The Bardeen solution arises from considering general relativity coupled to nonlinear electrodynamics [8, 9], while the Hayward solution is a modified Schwarzschild BH that incorporates a fundamental length scale [10]. These models exhibit de Sitter behavior near the center and asymptotically approach Schwarzschild spacetime at larger distances. A recent paper [11] presents a general regular solution with a de Sitter core within a gravitational collapse scenario. The stellar equation of state is shown to be of the polytropic type, resulting from the smooth matching of the interior and exterior geometries of the star, without imposing any a priori assumptions about the equation of state of the collapsing matter. The end product of gravitational collapse is a general static regular BH. This solution is characterized by the polytropic index of stellar matter; the Bardeen and Hayward BHs are special cases that correspond to specific polytropic indices [11].

In recent years, the study of BHs has moved beyond the traditional 4-dimensional framework to explore the intriguing realm of higher-dimensional spacetimes. This is due to theoretical advances in string theory and the potential for new physics at the TeV scale, suggesting the existence of large extra dimensions [12, 13].

In the context of general relativity, Tangherlini was the first to attempt to obtain a d -dimensional solution, which is a generalization of the Schwarzschild solution to higher dimensions [14]. Myers and Perry (MP) found exact solutions for a rotating BH in d dimensions [15]. Other studies of BHs in higher dimensions can be found in [16]. The generalization to a d -dimensional Bardeen BH has been studied in [17].

The shadow of a BH has been an active topic of interest in recent years due to the observations of M87* and the supermassive BH in the Milky Way galaxy Sgr A* [18, 19]. Therefore, by studying shadows theoretically and comparing them with the observations, we can test the theoretical models. Shadows can result from the presence of a massive compact object or a BH and are formed due to a strong gravitational field. Studies on the shadows of compact objects can be found in [20, 21, 22]. The shadow of d -dimensional Schwarzschild-Tangherlini (ST) BH is studied in [23] and other interesting topics regarding BHs' shadow in higher dimensions can be found in [24, 47].

Bardeen, Carter, and Hawking attempted to identify BHs as thermodynamic systems. They related changes in mass to the horizon area through a factor proportional to the surface gravity, which they called the first law of BH thermodynamics. This law is analogous to the first law of ordinary thermodynamics, with mass, surface gravity and horizon area playing the roles of energy, temperature and entropy, respectively [26]. Hawking solidified the analogy between temperature and surface gravity by showing that the creation of quantum particles leads to BH radiation [27].

Considering the BH as a thermodynamic system characterized by temperature and entropy makes studying its heat capacity crucial. Heat capacity indicates stability (instability) for positive (negative) values, and divergence signals a possible phase transition [28, 29]. Heat capacity also determines whether a BH is stable or unstable. If a BH were to absorb mass, negative heat capacity would mean its temperature decreases because the absorption rate would exceed the emission rate. Thus, the BH would grow, and the system would become unstable. However, the presence of other factors, such as magnetic charge, can stabilize the system [30].

Alongside studying the BH itself, an important question is whether such objects could result from stellar collapse. The classical model of collapse, developed by Oppenheimer, Snyder and Datt (OSD) [31, 32], smoothly connects the interior Friedmann-Lemaître-Robertson-Walker (FLRW) metric to the Schwarzschild metric, ultimately resulting in a singularity. Various proposals attempt to modify this scenario. One approach is to replace the Schwarzschild exterior with a regular BH containing a de Sitter core, which prevents the formation of a singularity due to repulsive effects related to the violation of the strong energy condition (SEC) [11]. Certain OSD model modifications introduce a bounce, thereby eliminating the singularity [33, 34]. In [35], the authors suggest that quantum effects may replace classical singularities with a bounce.

In this paper, we first introduce a general class of regular d -dimensional BHs with a de Sitter core. This is a generalization of the d -dimensional version of a general class of regular BHs proposed in [11]. We achieve this generalization by coupling the Einstein-Hilbert action to an appropriate nonlinear electrodynamics in which the magnetic charge acts as the free parameter ensuring regularity in each dimension. This extends [36], which was done for the Bardeen BH. Next, we study the energy conditions of this model, find the circular orbits, and identify the photon spheres and shadow. We perform an exact analysis of the photon spheres and a numerical analysis of the shadow for various values of the magnetic charge and spacetime dimension up to 11. Within the model, we study BH and compact object cases to determine the limits of photon sphere and shadow existence. Using a numerical approach, we also study the thermodynamic properties of the solution, including temperature, entropy, and heat capacity. Then, we examine the stability of the model and possible phase transitions. Finally, we generalize the OSD collapse scenario by smoothly joining a d -dimensional flat FLRW interior to a d -dimensional regular BH. We then study the evolution of the surface of the star, the apparent horizon and the event horizon.

The outline of this paper is as follows: Section 2 studies a general d -dimensional static spherically symmetric geometry and derives the corresponding Einstein equations. Section 3 introduces a family of d -dimensional regular BHs with a de Sitter core using an appropriate Lagrangian. We also compute the scalar curvature, horizons, extremal conditions, and energy conditions. Section 4 analyzes photon spheres using an exact approach and shadows using a numerical approach. Section 5 delves into the thermodynamics of BHs by studying surface gravity, temperature, and entropy using an exact approach. Additionally, we assess the thermodynamic stability of BHs by identifying potential phase transitions through heat capacity analysis. Section 6 presents the scenario of a star collapsing into a d -dimensional regular BH and studies the evolution of the star's surface, as well as the apparent and event horizons. Section 7 provides a summary and conclusion.

Throughout this paper, we assume the signature of the metric tensor is $(-, +, +, +)$. We use natural units in which $G = c = 1$. To simplify some calculations, we scale the variables by the mass parameter m and denote them with tildes, i.e., $\tilde{r} = r/m$.

2 d -dimensional static spherically symmetric geometry

We will consider a general static spherically symmetric spacetime in d dimensions with $g_{tt} = -1/g_{rr}$ as

$$ds^2 = -A_d(r)dt^2 + A_d^{-1}(r)dr^2 + r^2d\Omega_{d-2}^2, \quad (1)$$

where

$$d\Omega_{d-2}^2 = \sum_{i=1}^{d-2} \left[\prod_{j=2}^i \sin^2 \theta_{j-1} \right] d\theta_i^2, \quad (2)$$

is the line element of a $(d-2)$ -dimensional sphere [37, 38]. The Einstein equations then give [39, 40]

$$G^t_t = G^r_r = -\frac{(d-3)(d-2)}{2r^2} + \frac{(d-3)(d-2)}{2r^2}A_d(r) + \frac{(d-2)}{2r}A'_d(r) = 8\pi T^t_t = -8\pi\rho(r) = T^r_r = 8\pi p_r(r), \quad (3)$$

$$G^{\theta_i}_{\theta_i} = -\frac{(d-3)(d-4)}{2r^2} + \frac{(d-3)(d-4)}{2r^2}A_d(r) + \frac{(d-3)}{r}A'_d(r) + \frac{1}{2}A''_d(r) = 8\pi T^{\theta_i}_{\theta_i} = 8\pi p_t(r), \quad (4)$$

where $i \geq 1$ and a prime denotes differentiation with respect to the radial coordinate. Considering a perfect fluid as the source matter with the energy-momentum tensor (EMT) $T^\mu_\nu = \text{diag}[-\rho(r), p_r(r), p_t(r), \dots, p_t(r)]$, Eq. (3) can be integrated to

$$A(r) = 1 - \frac{m^{d-3}}{r^{d-3}} - \frac{2}{(d-2)r^{d-3}} \int \rho(r)r^{d-2}dr, \quad (5)$$

where m is an integration constant chosen so that $A(r) = 1$ when $\rho(r) = 0$ and $r \rightarrow \infty$. A comparison with the ST BH gives us [14]

$$m^{d-3} = \frac{16\pi M}{(d-2)\Omega_{d-2}}, \quad (6)$$

where M is the Arnowitt–Deser–Misner (ADM) mass and Ω_{d-2} is the volume of a unit $(d-2)$ -dimensional sphere

$$\Omega_{d-2} = \frac{2\pi^{\frac{d-1}{2}}}{\Gamma\left(\frac{d-1}{2}\right)}. \quad (7)$$

Combining (3) and (4) yields the relation between $p_t(r)$ and $\rho(r)$

$$-\rho(r) - \frac{1}{d-2}r\rho'(r) = p_t(r) \quad \Rightarrow \quad \rho(r)r^{d-2} = - \int r^{2-d}p_t(r)dr + C_1, \quad (8)$$

where C_1 is an arbitrary integration constant. Therefore, the relevant EMT must have the form $T^t_t = T^r_r$ and $T^{\theta_1}_{\theta_1} = T^{\theta_2}_{\theta_2}$ from (3) and (4). Furthermore, given the energy density function $\rho(r)$, the transverse pressures are given by (8).

In the following section, we introduce the appropriate nonlinear magnetic monopole Lagrangian and derive the exact form of the metric by applying (8).

3 A class of d -dimensional regular BHs

Our goal is to study a metric that describes a general class of regular d -dimensional BHs introduced in [11]. This class of geometries is parameterized by the free parameters m , q , and n . The latter is the polytropic index of stellar matter in the OSD collapse [11]. The metric in 4 dimensions is

$$ds^2 = -\left(1 - \frac{m}{r(1 + m^{\frac{3}{n}-1}q^2r^{-3/n})}\right)dt^2 + \left(1 - \frac{m}{r(1 + m^{\frac{3}{n}-1}q^2r^{-3/n})}\right)^{-1}dr^2 + r^2d\Omega_2^2, \quad (9)$$

where using (6), $m = 2M$ in 4 dimensions. This geometry describes a de Sitter core and as $r \rightarrow \infty$, the Schwarzschild solution is recovered. Known solutions for regular BHs with de Sitter cores include the Hayward and Bardeen metrics. Both metrics belong to the aforementioned class of spacetimes when the polytropic index takes the specific values $n = 1$

and $n = 3/2$, respectively. In addition to generalizing the metric (9) to d dimensions, we are interested in interpreting the sources of these geometries via nonlinear electrodynamics. Previous studies on the Bardeen BH have employed nonlinear electrodynamics to incorporate magnetic charge as a free parameter of the metric [36]¹. The Hayward BH contains a free parameter that acts as a fundamental length scale. For more information on studying the Hayward metric with nonlinear electrodynamics, see [42, 43]. As mentioned above, both BHs can be subsumed under a more general metric [11] and identified by specific values of the polytropic index.

Here, we consider the general class of regular BHs described by Eq. (9) and demonstrate that this class has a de Sitter core with nonlinear electrodynamics as its source. We also generalize the solution to a class of d -dimensional regular BHs with de Sitter cores. We begin with the action for nonlinear electrodynamics coupled to GR in d dimensions

$$\mathcal{A} = \frac{1}{16\pi} \int d^d x \sqrt{-g} [\mathcal{R} - 4\mathcal{L}(F)], \quad (10)$$

where \mathcal{R} is the Ricci scalar and F is the Maxwell scalar defined by contracting the Maxwell tensor

$$F = \frac{1}{4} F_{\mu\nu} F^{\mu\nu}, \quad F_{\mu\nu} = 2\nabla_{[\mu} A_{\nu]}. \quad (11)$$

The variation of the action (10) with respect to the metric yields

$$\mathcal{R}_{\mu\nu} - \frac{1}{2} g_{\mu\nu} \mathcal{R} = T_{\mu\nu}, \quad \nabla_\mu (\mathcal{L}_F F^{\mu\nu}) = 0, \quad \nabla_\mu (*F^{\mu\nu}) = 0, \quad (12)$$

where $\mathcal{L}_F = \partial\mathcal{L}/\partial F$. The EMT is

$$T_{\mu\nu} = 2(\mathcal{L}_F F_{\mu\nu}^2 - g_{\mu\nu} \mathcal{L}). \quad (13)$$

In 4 dimensions, substituting (9) into (3) yields the Lagrangian as a function of r

$$\mathcal{L}(r)|_{d=4} = \frac{3m^{\frac{3}{n}-1}}{2q^{2n}} \left(\frac{q^2 r^{-3/n}}{1 + m^{\frac{3}{n}-2} q^2 r^{-3/n}} \right)^{n+1}. \quad (14)$$

To find the Lagrangian in terms of F , we must use an ansatz. Assuming that the only non-zero component of the Maxwell tensor is $F_{\theta_1\theta_2}$, as in [36], the free parameter q plays the role of a magnetic charge. Thus, the Maxwell scalar would be $F = q^2/2r^4$. Consequently, we obtain the Lagrangian density in terms of the Maxwell scalar

$$\mathcal{L}(F)|_{d=4} = \frac{3m^{\frac{3}{n}-1}}{2q^{2n}} \left(\frac{\left(2Fq^{2(\frac{4n}{3}-1)}\right)^{\frac{3}{4n}}}{1 + m^{\frac{3}{n}-2} \left(2Fq^{2(\frac{4n}{3}-1)}\right)^{\frac{3}{4n}}} \right)^{n+1}. \quad (15)$$

This result reduces to the Bardeen Lagrangian for $n = 3/2$ [36, 41]². However, the Lagrangian (15) does not reduce to Maxwell's Lagrangian, $\mathcal{L}(F) = F$, and therefore, the Reissner–Nordström metric is not recovered in any limit. This is the main result of the above ansatz in which the monopole charge of a self–gravitating magnetic field is used instead of the Coulomb charge [36, 41].

To generalize the 4-dimensional Lagrangian (15) to higher dimensions, we must start by suggesting the Lagrangian density. Our suggestion for the appropriate form of the Lagrangian density in d -dimensions is as follows

$$\mathcal{L}(F) = \frac{(d-1)(d-2)m^{\frac{3(d-2)}{2n}-1}}{4q^{\frac{2n}{3}(d-1)}} \left[\frac{\left(2Fq^{2(\frac{2n}{3}(d-2)-(d-3))}\right)^{\frac{3}{4n}}}{1 + m^{\left(\frac{d-2}{2}\right)\left(\frac{3}{n}-2\right)} \left(2Fq^{2(\frac{2n}{3}(d-2)-(d-3))}\right)^{\frac{3}{4n}}} \right]^{\frac{2n}{3}\frac{d-1}{d-2}+1}, \quad (16)$$

where n is an arbitrary positive parameter that plays the role of the polytropic index in the aforementioned collapse scenario and m is the parameter introduced in (6) that is related to the ADM mass. The cases $n = 1$ and $n = 3/2$ correspond to the nonlinear Lagrangians sourcing the Hayward and Bardeen BHs.

From Eqs. (16) and (13), we find that

$$T^t_t = T^r_r = T^{\theta_\ell}_{\theta_\ell} = -2\mathcal{L}(F), \quad (17)$$

¹There is also a study that considers an electric source for the Bardeen BH, but that is not our focus here [41].

²Using (13) and the metric (9), the Lagrangian (15) satisfies both (3) and (4) in 4 dimensions.

where $\ell \geq 3$, and

$$T^{\theta_1}{}_{\theta_1} = T^{\theta_2}{}_{\theta_2} = 2(2F\mathcal{L}_F - \mathcal{L}). \quad (18)$$

Substituting Eqs. (17) and (18) into Eq. (8) yields

$$4F + \frac{2}{d-2}F' = 0 \quad \rightarrow \quad F = \frac{C_2}{r^{2(d-2)}}, \quad (19)$$

where C_2 is the integration constant. On the other hand, the Maxwell field tensor describing a magnetic charge in d dimensions is [17]

$$F_{\mu\nu} = 2\delta_{[\mu}^{\theta_{d-3}}\delta_{\nu]}^{\theta_{d-2}}\frac{q^{d-3}}{r^{d-4}}\sin\theta_{d-3}\left[\prod_{j=1}^{d-4}\sin^2\theta_j\right], \quad (20)$$

which gives the Maxwell scalar as

$$F = \frac{q^{2(d-3)}}{2r^{2(d-2)}}. \quad (21)$$

Comparing this with (19) yields the constant C_2 . We can then substitute (21) into (16) to obtain the radial dependence of the Lagrangian

$$\mathcal{L}(r) = \frac{(d-1)(d-2)q^{d-2}m^{\frac{3(d-2)}{2n}-1}}{4\left(r^{\frac{3(d-2)}{2n}} + m^{\left(\frac{d-2}{2}\right)\left(\frac{3}{n}-2\right)}q^{d-2}\right)^{\frac{2n}{3}\frac{d-1}{d-2}+1}}. \quad (22)$$

Using this expression, the metric component $A_d(r)$ can be found from (17), and (5) as

$$A_d(r) = 1 - \frac{m^{d-3}}{r^{d-3}}\left(1 + \frac{m^{\left(\frac{d-2}{2}\right)\left(\frac{3}{n}-2\right)}q^{d-2}}{r^{\frac{3(d-2)}{2n}}}\right)^{\frac{-2n}{3}\frac{(d-1)}{(d-2)}}, \quad (23)$$

where the integration constant resulting from (5) is chosen so that the above solution agrees with the ST solution for $q = 0$. Eqs. (22) and (23) are consistent with d -dimensional Bardeen BH spacetime (i.e., $n = 3/2$) [17] and also with 4-dimensional Hayward (i.e., $n = 1$) [10]. The behavior of the metric component $A_d(r)$ with respect to the radius is plotted in Fig. 1. As the dimension increases, the minima of $A_d(r)$ become more separated, while the maxima converge. Increasing the polytropic index enhances this behavior. From metric component (23), we see that $A_d(r)$ asymptotically approaches

$$A_d(r) \approx 1 - \frac{m^{d-3}}{r^{d-3}}\left[1 - \left(\frac{2n}{3}\left(\frac{d-1}{d-2}\right)\frac{m^{\left(\frac{d-2}{2}\right)\left(\frac{3}{n}-2\right)}q^{d-2}}{r^{\frac{3(d-2)}{2n}}}\right) + \text{terms of higher orders } \frac{1}{r}\right], \quad r \rightarrow \infty, \quad (24)$$

$$A_d(r) \approx 1 - \frac{m^{d-3}r^2}{\left(m^{\left(\frac{d-2}{2}\right)\left(\frac{3}{n}-2\right)}q^{d-2}\right)^{\frac{2n}{3}\frac{d-1}{d-2}}}\left[1 - \frac{2n}{3}\frac{d-1}{d-2}\frac{r^{\frac{3}{2n}(d-2)}}{m^{\left(\frac{d-2}{2}\right)\left(\frac{3}{n}-2\right)}q^{d-2}} + \text{terms of higher orders } r\right], \quad r \rightarrow 0. \quad (25)$$

Thus, despite the presence of the magnetic charge q , Eq. (24) and Fig. 1 show that the solution increasingly resembles the ST solution as the radius increases. Conversely, (25) shows that the magnetic charge has a greater influence on smaller radii.

For the line element (1) with the metric component (23), the Ricci scalar is given by

$$\mathcal{R} = \frac{1}{r^2}\left[(d-3)(d-2)(1-A_d(r)) - 2(d-2)rA'_d(r) - r^2A''_d(r)\right], \quad (26)$$

$$= \frac{(d-1)m^{\frac{3(d-2)}{2n}-1}q^{d-2}}{\left(m^{\left(\frac{d-2}{2}\right)\left(\frac{3}{n}-2\right)}q^{d-2} + r^{\frac{3(d-2)}{2n}}\right)^{\frac{2n(d-1)}{3(d-2)}+2}}\left(m^{\left(\frac{d-2}{2}\right)\left(\frac{3}{n}-2\right)}dq^{d-2} - \frac{3d-2(n+3)}{2n}r^{\frac{3(d-2)}{2n}}\right). \quad (27)$$

For $q \neq 0$, the scalar curvature is obviously finite at $r = 0$.

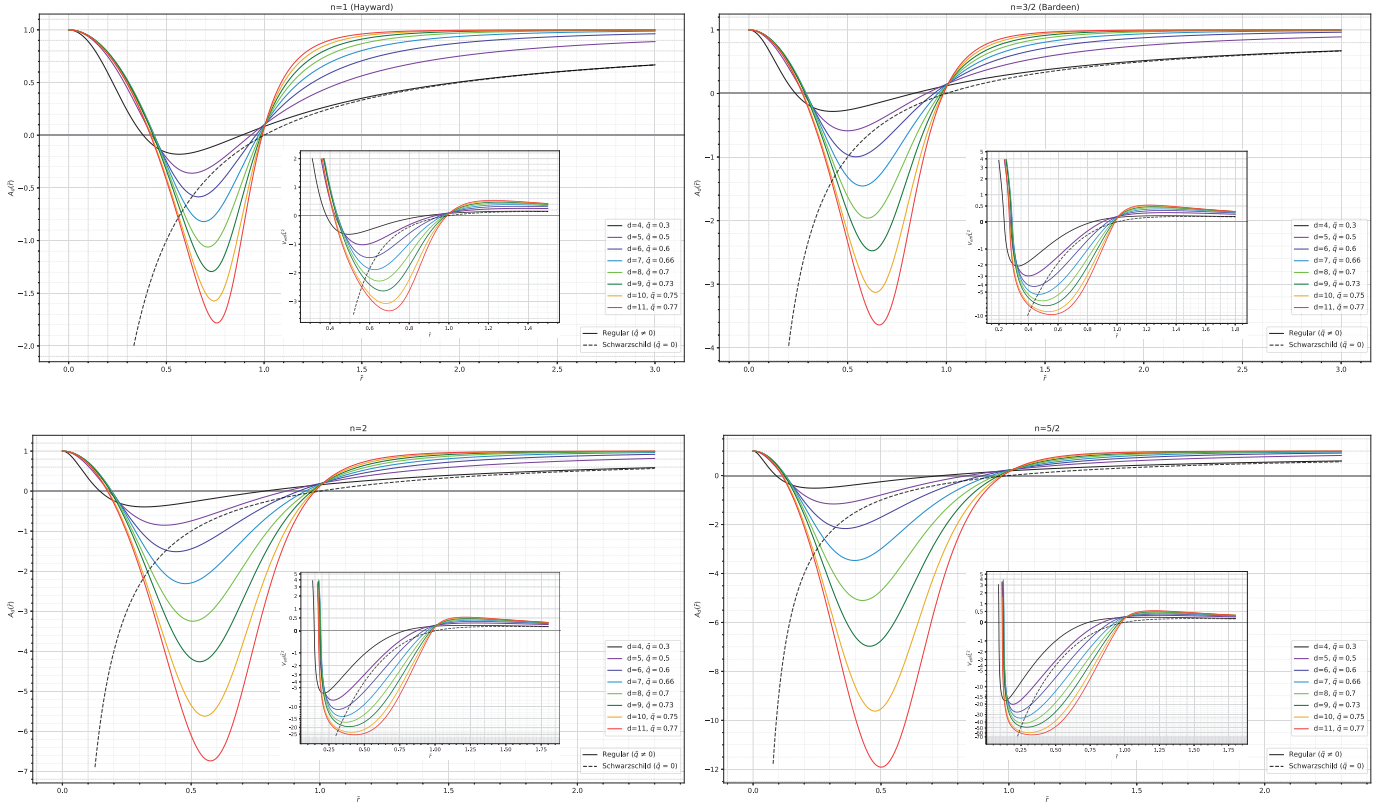


Figure 1: The plot of $A_d(\tilde{r})$ and the corresponding effective potential for a massless particle as a function of radius (\tilde{r} is scaled by m as $\tilde{r} = r/m$) for different dimensions and for the cases $n = 1$ (i.e., Hayward), $n = 3/2$ (i.e., Bardeen), $n = 2$ and $n = 5/2$. The magnetic charge q is set to different values in each dimension to make the plots comparable. The value of the rescaled magnetic charge \tilde{q} is chosen so that the BH has two distinct roots. This ensures that the BH is neither extremal nor horizonless. The dashed line represents the Schwarzschild BH in 4 dimensions. We have omitted other dimensions for the ST BH plot due to the indistinguishability of the curves. The same \tilde{q} values are used for the effective potential plot.

3.1 Horizons

The horizons are the roots of $A_d(r)$, so from (23), we have

$$\mathfrak{R}_h^{3-d} + \mathfrak{R}_h^2 m^{\left(\frac{d-2}{2}\right)\left(\frac{3}{n}-2\right)} q^{d-2} - m^{\frac{3}{2n} \frac{(d-2)(d-3)}{(d-1)}} = 0, \quad (28)$$

where $\mathfrak{R}_h = r_h^{-\frac{3(d-2)}{2n(d-1)}}$ and r_h is the radius of the horizon(s). The order of the algebraic equation (28) depends on d . This emphasizes the importance of specifying the dimension in order to analytically find the horizon radius. Mathematically, for odd dimensions up to $d = 9$, Eq. (28) is analytically solvable for r_h . Some exact solutions are examined in Appendix A. For the general dimension, Eq. (28) can have two real roots, one real root, or no real roots. This can be seen in the zero points of $A_d(r)$ in Fig. 1.

Although the horizon equation cannot be solved for r_h in any dimension, it can be solved analytically for q as

$$q = m^{1-\frac{3}{2n}} r_h^{\frac{3}{2n}} \left(\left(\frac{m^{d-3}}{r_h^{d-3}} \right)^{\frac{3(d-2)}{2(d-1)n}} - 1 \right)^{\frac{1}{d-2}}, \quad (29)$$

which can be written in terms of dimensionless quantities, i.e., $\tilde{r} = r/m$ and $\tilde{q} = q/m$, as

$$\tilde{q} = \tilde{r}_h^{\frac{3}{2n}} \left(\left(\tilde{r}_h^{d-3} \right)^{-\frac{3(d-2)}{2n(d-1)}} - 1 \right)^{\frac{1}{d-2}}. \quad (30)$$

The extremal case with only one real root can be found analytically using the condition $A_d(\tilde{r}_{\text{ext}}) = A'_d(\tilde{r}_{\text{ext}}) = 0$.

These equations give the extremality condition and also the radius of the extremal horizon, respectively as

$$\tilde{q}_{\text{ext}} = \left(\frac{d-3}{2} \right)^{\frac{1}{d-2}} \left(\frac{2}{d-1} \right)^{\frac{d-1}{(d-3)(d-2)}}, \quad (31)$$

$$\tilde{r}_{\text{ext}} = \left(\frac{2}{d-1} \right)^{\frac{2n(d-1)}{3(d-2)(d-3)}}. \quad (32)$$

The above equations show that the value of \tilde{q} for extremality is independent of the polytropic index n , while the extremal radius depends on it. According to Eqs. (31) and (32), the scaled radius of the extremal horizon and the corresponding scaled charge approach unity as d approaches infinity. This shows that the rate of change of \tilde{q}_{ext} and \tilde{r}_{ext} decreases with increasing dimensions. In each dimension, \tilde{q}_{ext} is the maximum charge value. For larger values, the horizon equation (28) has no roots, thus, the metric (23) represents a compact object without a horizon.

3.2 Energy conditions

According to Einstein's equations (3) and (4), we discuss the energy conditions using the EMT in the form of $T^{\mu}_{\nu} = \text{diag}[-\rho(r), p_r(r), p_t(r), \dots, p_t(r)]$. For this form of the EMT, weak energy condition (WEC), null energy condition (NEC), dominant energy condition (DEC), and strong energy condition (SEC) are expressed as [44]

- (i) $\text{WEC}_{1,2}(r) = \text{NEC}_{1,2}(r) : \rho + p_i \geq 0$,
- (ii) $\text{WEC}_3(r) = \text{DEC}_1(r) : \rho \geq 0$,
- (iii) $\text{SEC}(r) = (d-3)\rho + p_r + (d-2)p_t \geq 0$
- (iv) $\text{DEC}_{2,3}(r) : \rho + p_i \geq 0$, and $\rho - p_i \geq 0$

where $i = r, t$ denotes the radial and tangential pressures. Using Einstein's equations (3) and (4)

$$8\tilde{\pi}\tilde{\rho}(\tilde{r}) = -8\pi\tilde{p}_r(\tilde{r}) = \frac{(d-1)(d-2)}{2\tilde{r}^{d-1}}\tilde{q}^{d-2}\tilde{r}^{-\frac{3(d-2)}{2n}}\left(\tilde{q}^{d-2}\tilde{r}^{-\frac{3(d-2)}{2n}} + 1\right)^{-\frac{2(d-1)n}{3(d-2)}-1}, \quad (33)$$

$$8\pi\tilde{p}_t(\tilde{r}) = \frac{(d-1)}{4n\tilde{r}^{d-1}}\tilde{q}^{d-2}\tilde{r}^{-\frac{3(d-2)}{2n}}\left(\tilde{q}^{d-2}\tilde{r}^{-\frac{3(d-2)}{2n}} + 1\right)^{-\frac{2(d-1)n}{3(d-2)}-2}\left((3d+2n-6) - 2(d-2)n\tilde{q}^{d-2}\tilde{r}^{-\frac{3(d-2)}{2n}}\right). \quad (34)$$

It is evident that the $\text{WEC}_{1,2}$ and $\text{NEC}_{1,2}$ are satisfied everywhere because $\tilde{\rho} + \tilde{p}_r = 0$. Also, since \tilde{q} and n are positive, $\rho \geq 0$ and therefore, the WEC_3 and DEC_1 are satisfied as well. Additionally,

$$\tilde{\rho} + \tilde{p}_t = \frac{(d-1)(2(d-1)n + 3(d-2))}{32\pi n\tilde{r}^{d-1}}\tilde{q}^{d-2}\tilde{r}^{-\frac{3(d-2)}{2n}}\left(\tilde{q}^{d-2}\tilde{r}^{-\frac{3(d-2)}{2n}} + 1\right)^{-\frac{2(d-1)n}{3(d-2)}-2}, \quad (35)$$

is always positive. Thus, the $\text{WEC}_{1,2}$ and consequently, the $\text{NEC}_{1,2}$ hold everywhere. Since $\tilde{\rho} + \tilde{p}_i \geq 0$, violating DEC_2 , means violating $\tilde{\rho} - \tilde{p}_r \geq 0$, which is satisfied everywhere since both $\tilde{\rho}$ and $-\tilde{p}_r$ are positive. Therefore, only the tangential component must be checked. A simple calculation also reveals that

$$\begin{aligned} \text{DEC}_3(\tilde{r}) = \tilde{\rho} - \tilde{p}_t &= \frac{(d-1)\tilde{q}^{d-2}\tilde{r}^{-\frac{3(d-2)}{2n}}}{32\pi n\tilde{r}^{d-1}}\left(\tilde{q}^{d-2}\tilde{r}^{-\frac{3(d-2)}{2n}} + 1\right)^{-\frac{2(d-1)n}{3(d-2)}-2} \\ &\times \left(4(d-2)n\tilde{q}^{d-2}\tilde{r}^{-\frac{3(d-2)}{2n}} + (d(2n-3) - 6n + 6)\right) \geq 0 \end{aligned} \quad (36)$$

Only the last parenthesis can be negative. It is positive if

$$n \geq \frac{3(d-2)}{2(d-3)} \quad (37)$$

In this case, DEC_3 is satisfied everywhere. Otherwise, it is only satisfied for

$$\tilde{r} \leq \left(\frac{4n(d-2)\tilde{q}^{d-2}}{3(d-2) - 2n(d-3)} \right)^{\frac{2n}{3(d-2)}} \equiv \tilde{r}_{\text{DEC}}. \quad (38)$$

To satisfy the SEC, it is required that

$$\begin{aligned} & \frac{(d-2)(d-1)}{32\pi n\tilde{r}^{d-1}}\tilde{q}^{d-2}\tilde{r}^{-\frac{3(d-2)}{2n}}\left(\tilde{q}^{d-2}\tilde{r}^{-\frac{3(d-2)}{2n}}+1\right)^{-\frac{2(d-1)n}{3(d-2)}-2} \\ & \times\left(2(d-3)n+3(d-2)-4n\tilde{q}^{d-2}\tilde{r}^{-\frac{3(d-2)}{2n}}\right)\geq 0, \end{aligned} \quad (39)$$

holds. Only the last expression in parentheses can be negative. Therefore, the SEC is satisfied if

$$\tilde{r}\geq\left(\frac{4n\tilde{q}^{d-2}}{2n(d-3)+3(d-2)}\right)^{\frac{2n}{3(d-2)}}\equiv\tilde{r}_{\text{SEC}}. \quad (40)$$

From (38) and (40), we get

$$\frac{\tilde{r}_{\text{DEC}}}{\tilde{r}_{\text{SEC}}}=\left(\frac{(d-2)(3(d-2)+2n(d-3))}{3(d-2)-2n(d-3)}\right)^{\frac{2n}{3(d-2)}}. \quad (41)$$

For a given d and n , it is clear that $\tilde{r}_{\text{DEC}}\geq\tilde{r}_{\text{SEC}}$. The SEC and DEC_3 are plotted as a function of radius in Fig. 2. According to (38) and (40), these energy conditions can be violated at certain radii. Additionally, if the polytropic indices and dimensions satisfy (37), then there is no DEC_3 violation.

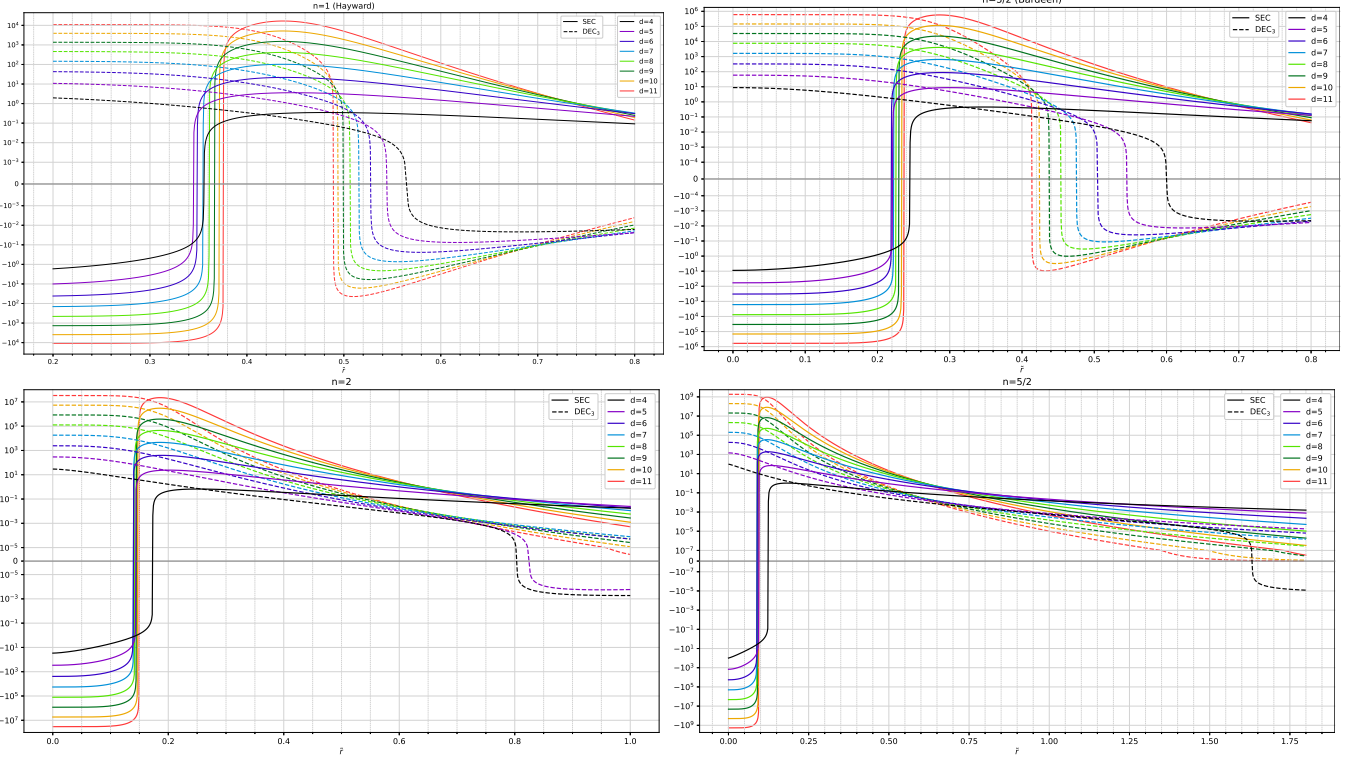


Figure 2: SEC and DEC_3 as a function of the dimensionless radius for different polytropic indices and dimensions. The solid and dashed lines represent SEC and DEC_3 , respectively. All other energy conditions are satisfied.

4 Null geodesics

In this section, we will find the null circular orbits of the metric component (23). The first step is to write the Lagrangian as

$$\mathcal{L}=\frac{1}{2}g_{\alpha\beta}\dot{x}^\alpha\dot{x}^\beta=\frac{1}{2}\left[-A_d(r)\dot{t}^2+A_d(r)^{-1}\dot{r}^2+r^2\sum_{i=1}^{d-2}\left[\prod_{j=2}^i\sin^2\theta_{j-1}\right]\dot{\theta}_i^2\right], \quad (42)$$

where the dot indicates differentiation with respect to the affine parameter. The canonically conjugate momentum $P_\mu = \partial \mathcal{L} / \partial \dot{x}^\mu$ can be calculated as [23]

$$P_t = -A_d(r)\dot{t}, \quad (43)$$

$$P_r = A_d(r)^{-1}\dot{r}, \quad (44)$$

$$P_{\theta_i} = r^2 \sum_{i=1}^{d-3} \prod_{j=1}^{i-1} \sin^2 \theta_j \dot{\theta}_{d-3}, \quad i = 1, 2, \dots, d-3, \quad (45)$$

$$P_{\theta_{d-2}} = r^2 \prod_{i=1}^{d-3} \sin^2 \theta_i \dot{\theta}_{d-2}, \quad (46)$$

where θ_{d-2} is the last tangent coordinate of spacetime. Due to the spherical symmetry of the gravitational field, we can restrict ourselves to $\theta_i = \pi/2$ (except for θ_{d-2}), without loss of generality. The conserved quantities along the geodesic, E and L , are given by the following Euler-Lagrange equations

$$t : -A_d(r)\dot{t} = E, \quad (47)$$

$$\theta_{d-2} : r^2 \prod_{i=1}^{d-3} \sin^2 \theta_i \dot{\theta}_{d-2} = r^2 \dot{\theta}_{d-2} = L, \quad (48)$$

which allows us to rewrite the Lagrangian (42) as

$$\mathcal{L} = \frac{\epsilon}{2} = -\frac{E^2}{2A_d(r)} + \frac{\dot{r}^2}{2A_d(r)} + \frac{L^2}{2r^2}. \quad (49)$$

The parameter ϵ for the timelike and null geodesics is set to -1 and 0 , respectively. Multiplying (49) by $A_d(r)$ and rearranging the terms yields

$$E^2 + \epsilon = \dot{r}^2 - \epsilon(A_d(r) - 1) + \frac{A_d(r)L^2}{r^2}. \quad (50)$$

For null geodesics (i.e., $\epsilon = 0$)

$$E^2 = \dot{r}^2 + V_{\text{eff}}, \quad \text{where} \quad V_{\text{eff}} = \frac{A_d(r)L^2}{r^2}. \quad (51)$$

The effective potential, normalized to L^2 , is plotted in Fig. 1 for different values of dimension and \tilde{q} . This potential tends to infinity as $r \rightarrow 0$ and approaches zero for large values of r .

4.1 Photon spheres

Here we focus on photon spheres. For a null circular geodesic, $\dot{r} = 0$ which yields $E^2 = V_{\text{eff}}$ using Eq. (51). To determine the radius of the photon sphere, we require $\ddot{r} = 0$ which is equivalent to $dV_{\text{eff}}/dr = 0$. The two conditions mentioned above give the following equations, which describe the photon spheres of the geometry (23)

$$\dot{r} = 0 \quad \Rightarrow \quad \frac{\tilde{E}^2}{\tilde{L}^2} = \frac{A_d(\tilde{r})}{\tilde{r}^2} = \frac{1}{\tilde{r}^2} \left(1 - \frac{1}{\tilde{r}^{d-3}} \left(1 + \frac{\tilde{q}^{d-2}}{\tilde{r}^{\frac{3(d-2)}{2n}}} \right)^{-\frac{(d-1)(2n)}{3(d-2)}} \right), \quad (52)$$

$$\frac{\tilde{V}'_{\text{eff}}}{\tilde{L}^2} = \frac{A'_d(\tilde{r})}{\tilde{r}^2} - \frac{2A_d(\tilde{r})}{\tilde{r}^3} = 0 \quad \Rightarrow \quad \frac{2\tilde{r}^{d-3}}{d-1} = \left(1 + \frac{\tilde{q}^{d-2}}{\tilde{r}^{\frac{3}{2n}(d-2)}} \right)^{-\frac{2n(d-1)}{3(d-2)}-1}. \quad (53)$$

Combining these equations leads to the following equation for the radius of the photon sphere, \tilde{r}_{PS}

$$\tilde{r}_{\text{PS}} = \left(\frac{2}{d-1} \right)^{\frac{2n(d-1)}{3(d-2)(d-3)}} \left(1 - \frac{E^2 \tilde{r}_{\text{PS}}^2}{L^2} \right)^{-\frac{2n(d-1)}{(d-2)(d-3)} - \frac{1}{d-3}}. \quad (54)$$

The right-hand side of the above equation is the product of two factors. The first factor is the radius of the extremal horizon, as given by (32) and the second factor is greater than one. From this, we deduce that $\tilde{r}_{\text{PS}} \geq \tilde{r}_{\text{ext}}$, i.e., the photon sphere is always outside the outer horizon, unless

$$\frac{\tilde{E}^2}{\tilde{L}^2} = \frac{1}{\tilde{r}^2} - \frac{1}{\tilde{r}^{d-3}} \left(1 + \left(\frac{2}{d-1} \right)^{\frac{d-1}{d-3}} \tilde{r}^{-\frac{3(d-2)}{2n}} \right)^{-\frac{2(d-1)n}{3(d-2)}}, \quad (55)$$

in which case the photon sphere coincides with the extremal horizon.

Now, we want to find the radius of the photon sphere for which the extreme value of \tilde{q} occurs. According to Eq. (53), on the photon sphere, $A'_d = 2A_d/r$. This gives $\tilde{q} = \tilde{q}(\tilde{r}_{\text{ph}})$, and then we can find its extremum. To do so, we write Eq. (53) as

$$A'(\tilde{r}_{\text{PS}}, \tilde{q}(\tilde{r}_{\text{PS}})) = \frac{2}{\tilde{r}_{\text{PS}}} A(\tilde{r}_{\text{PS}}, \tilde{q}(\tilde{r}_{\text{PS}})). \quad (56)$$

Calculating the total derivative of the above equation with respect to the radius of the photon sphere yields

$$\frac{\partial \tilde{q}}{\partial \tilde{r}} = -\tilde{V}_{\text{eff}}'' \left(A(\tilde{r}_{\text{PS}}, \tilde{q}(\tilde{r}_{\text{PS}})) - \frac{2}{\tilde{r}} \frac{\partial A(\tilde{r}_{\text{PS}}, \tilde{q}(\tilde{r}_{\text{PS}}))}{\partial \tilde{q}} \right)^{-1}, \quad (57)$$

and setting $\partial \tilde{q} / \partial \tilde{r}_{\text{PS}} = 0$, we obtain

$$A''_d(\tilde{r}_{\text{PS}}, \tilde{q}(\tilde{r}_{\text{PS}})) = \frac{2A'_d(\tilde{r}_{\text{PS}}, \tilde{q}(\tilde{r}_{\text{PS}}))}{\tilde{r}_{\text{PS}}} - \frac{2A_d(\tilde{r}_{\text{PS}}, \tilde{q}(\tilde{r}_{\text{PS}}))}{\tilde{r}_{\text{PS}}} = \frac{2A_d(\tilde{r}_{\text{PS}}, \tilde{q}(\tilde{r}_{\text{PS}}))}{\tilde{r}_{\text{PS}}^2}. \quad (58)$$

Eq. (58) is actually $\tilde{V}_{\text{eff}}'' = 0$, which has been evaluated at the photon sphere¹ and yields the extremum of \tilde{q}_{PS} in Eq. (53). For the corresponding radius, the two photon spheres coincide, forming a degenerate photon sphere. Its radius and charge are given by

$$\tilde{q}_{\text{PS, deg}} = \left(\frac{d-1}{2} \right)^{\frac{3}{2n(d-3)}} \left(\frac{3d+4n-6}{2n(d-3)} \right)^{\frac{1}{2-d}} \left(\frac{2n(d-3)}{3d+4n-6} + 1 \right)^{\frac{2n(1-d)+3(2-d)}{2n(d-3)(d-2)}}, \quad (59)$$

$$\tilde{r}_{\text{PS, deg}} = \left(\frac{d-1}{2} \right)^{\frac{1}{d-3}} \left(\frac{2n(d-3)}{3d+4n-6} + 1 \right)^{\frac{2n(1-d)+3(2-d)}{3(d-2)(d-3)}}. \quad (60)$$

To understand how $\tilde{r}_{\text{PS, deg}}$ behaves with respect to n , it is sufficient to consider

$$\frac{d\tilde{r}_{\text{PS, deg}}}{dn} = -\tilde{r}_{\text{PS, deg}} \left(\frac{2}{3d+4n-6} + \frac{2(d-1) \ln \left(\frac{2(d-3)n}{3d+4n-6} + 1 \right)}{3(d-3)(d-2)} \right). \quad (61)$$

Since $d > 4$ and $n \geq 0$, the expression in parentheses is always positive, so $d\tilde{r}_{\text{PS, deg}}/dn < 0$. In other words, an increase in the polytropic index causes a decrease in $\tilde{r}_{\text{PS, deg}}$. For $\tilde{q} = \tilde{q}_{\text{PS, deg}}$, Eq. (53) has only one positive real root, which corresponds to a horizonless compact object with a degenerate photon sphere. For any value of $\tilde{q} > \tilde{q}_{\text{PS, deg}}$, Eq. (53) has no acceptable roots, and thus no photon spheres. Conversely, for $\tilde{q} < \tilde{q}_{\text{PS, deg}}$, this equation has at most two real positive roots. In both cases, as previously mentioned, the photon spheres are always outside the extremal horizon. See Fig. 1 for clarification.

We can analyze the stability of photon spheres by examining \tilde{V}_{eff}'' on the photon sphere. Negative and positive values indicate unstable and stable photon spheres, respectively. Substituting (23) into (57) reveals that the expression in parentheses is always negative. Therefore $\partial \tilde{q} / \partial \tilde{r} < 0$ (or equivalently $\tilde{r}_{\text{PS}} > \tilde{r}_{\text{PS, deg}}$) corresponds to $\tilde{V}_{\text{eff}}'' < 0$ meaning the photon sphere is unstable, and $\partial \tilde{q} / \partial \tilde{r} > 0$ (or equivalently, $\tilde{r}_{\text{PS}} < \tilde{r}_{\text{PS, deg}}$) corresponds to $\tilde{V}_{\text{eff}}'' > 0$, meaning the photon sphere is stable. When $\partial \tilde{q} / \partial \tilde{r} = 0$, i.e., $\tilde{q} = \tilde{q}_{\text{PS, deg}}$, there is a marginally unstable photon sphere at $\tilde{r}_{\text{PS, deg}}$.

For $\tilde{q} = 0$, \tilde{V}_{eff}' has a single root at $\tilde{r} = \tilde{r}_{\text{PS, ST}}$. This corresponds to the single photon sphere of a ST BH. The radius of the photon sphere, together with the corresponding effective potential, can be calculated as

$$\tilde{r}_{\text{PS, ST}} = \left(\frac{d-1}{2} \right)^{\frac{1}{d-3}}, \quad \tilde{V}_{\text{eff, ST}}|_{\tilde{r}_{\text{PS, ST}}} = \tilde{L}^2 \left(\frac{d-3}{d-1} \right) \left(\frac{2}{d-1} \right)^{\frac{2}{d-3}}, \quad (62)$$

¹This can easily be seen by calculating the second derivative of Eq. (51) on the photon sphere.

where $\tilde{V}_{\text{eff}}''|_{\tilde{r}_{\text{PS, ST}}} < 0$ indicating an unstable photon sphere, as expected. At $d = 4$ and $\tilde{q} = 0$, we recover the Schwarzschild maximum of the effective potential $\tilde{V}_{\text{eff, S}}|_{\tilde{r}_{\text{PS, S}}} = 4\tilde{L}^2/27$ with a radius $\tilde{r}_{\text{PS, S}} = 3/2$ ¹.

Fig. 3 shows the schematic behavior of the horizons, photon spheres and their stability. Using Fig. 3 and noting Eq. (54), Fig. 4 plots the BH photon spheres (BHPS) and compact object photon spheres (COPS) as well as the outer and inner horizons (30), for different dimensions and polytropic indices.

For the BH case, whether extremal or non-extremal, there is an unstable outer photon sphere. For a compact object, there are two photon spheres: the outer one is unstable and the inner one is stable. For a given d and n , $\tilde{q}_{\text{PS, deg}} > \tilde{q}_{\text{ext}}$ and $\tilde{r}_{\text{PS, deg}} > \tilde{r}_{\text{ext}}$, and for $\tilde{q} = \tilde{q}_{\text{PS, deg}}$, there is one degenerate photon sphere. For $\tilde{q} > \tilde{q}_{\text{PS, deg}}$, there are no photon spheres.

4.2 Shadows

A photon emitted from a source toward a spherically symmetric BH or compact object can have two fates depending on its energy and angular momentum. The photon may be captured by the BH's or compact object's gravitational field or it can escape and go to infinity. The shadow corresponds to the region where the light rays are captured by the BH or compact object. The boundary of the shadow consists of light rays that neither escape to infinity nor fall into the BH. Instead, they approach a circular orbit, i.e., the photon sphere. It is the locus of the trapped photons and is defined by the roots of $\dot{r} = \ddot{r} = 0$, as seen in 4.1.

To determine the shadow's size [45], we assume a static observer at a given radius sends light rays into the past. Then, we calculate the angle between the light rays' trajectories that asymptotically approach the photon sphere and the radial direction. A straightforward calculation yields [46]

$$\sin \alpha_{\text{Sh}} = \frac{r_{\text{PS}}}{r_{\text{o}}} \sqrt{\frac{A_{r_{\text{o}}}}{A_d(r_{\text{PS}})}}, \quad (63)$$

where r_{o} corresponds to the observer's position. By moving the observer away from the BH or compact object and substituting (23) and (54) in the above²

$$\sin \alpha_{\text{Sh}}|_{\tilde{r}_{\text{o}} \rightarrow \infty} \approx \frac{\tilde{r}_{\text{PS}}}{\sqrt{A_d(\tilde{r}_{\text{PS}})}} = \frac{\left(\frac{2}{d-1}\right)^{\frac{2n(d-1)}{3(d-2)(d-3)}}}{(1 - b^{-2}\tilde{r}_{\text{PS}}^2)^{\frac{2n(d-1)}{(d-2)(d-3)} + \frac{1}{d-3}}} \left(1 - \frac{1}{\tilde{r}_{\text{PS}}^{d-3}} \left(1 + \frac{\tilde{q}^{d-2}}{\tilde{r}_{\text{PS}}^{2n}}\right)^{\frac{-2n}{3(d-2)}}\right)^{-1/2}, \quad (64)$$

where $b = L/E$ is the impact parameter. For the case of $\tilde{q} = 0$, i.e., ST BH, using (62) and (64) yields the radius of the shadow

$$\tilde{r}_{\text{Sh, ST}} = \left(\frac{d-1}{2}\right)^{\frac{1}{d-3}} \sqrt{\frac{d-1}{d-3}}. \quad (65)$$

Note that according to (59), the shadow exists only for $0 \leq \tilde{q} \leq \tilde{q}_{\text{deg}}$. At $\tilde{q} = \tilde{q}_{\text{deg}}$, the shadow coincides with the photon sphere, and for $\tilde{q} > \tilde{q}_{\text{deg}}$, the photon sphere and thus, the shadow disappears³.

The size of the shadow for different values of \tilde{q} , up to the maximum \tilde{q}_{deg} that shadows can exist, is calculated numerically and listed in table 1. As q , the dimension d , or the polytropic index n increases, the shadow's size decreases. Therefore, for a given d and n , $\tilde{q} = \tilde{q}_{\text{deg}}$ gives the minimum shadow radius and for a Schwarzschild BH in 4 dimensions, the BH shadow would be maximally sized.

To compare the 4-dimensional results with the observations, the shadow radii of $M87^*$ and SgrA^* are used here. These are given by $r_{\text{Sh}}/M \approx 5.5 \pm 0.8$ and $4.21 \lesssim r_{\text{Sh}}/M \lesssim 5.56$, respectively [48, 49]. Note that the results in table 1 should be written in terms of the ADM mass using Eq. (6). In 4 dimensions, this means multiplying the values in table 1 by two. Figure 5 plots the shadow radius of the regular class of BH spacetime (23) in 4 dimensions (i.e., Eq. (9)) compared to that of SgrA^* and $M87^*$. Solutions with lower \tilde{q} and n are more consistent with observational data than those with higher \tilde{q} and n .

¹Note that, in 4 dimensions, $V_{\text{eff}}|_{\tilde{r}_{\text{PS}}}$ and $r_{\text{PS, S}}$ for Schwarzschild spacetime are $L^2/27M^2$ and $3M$, respectively. These values can be related to the tilde notation using (6) by substituting $\tilde{m} = 2M$.

²It should be mentioned that the shadow of the d -dimensional BH is defined on the 2-dimensional surface corresponding to the observer. Accordingly, the shadow of the 5-dimensional rotating Myers-Perry BH has also been studied on a 2-dimensional surface, as discussed in [47].

³Alternatively, consider a photon arriving from infinity, which will only be deflected if $\tilde{E}^2 < \tilde{V}_{\text{eff}}|_{\tilde{r}_{\text{PS}}}$. Otherwise, it would be captured by the BH or compact object. For a photon to be deflected rather than captured, its impact parameter must satisfy $b > \tilde{L}/(\tilde{V}_{\text{eff}}|_{\tilde{r}_{\text{PS}}})^{1/2}$. For $\tilde{q} > \tilde{q}_{\text{deg}}$, there are no extrema in \tilde{V}_{eff} and hence no \tilde{r}_{PS} .

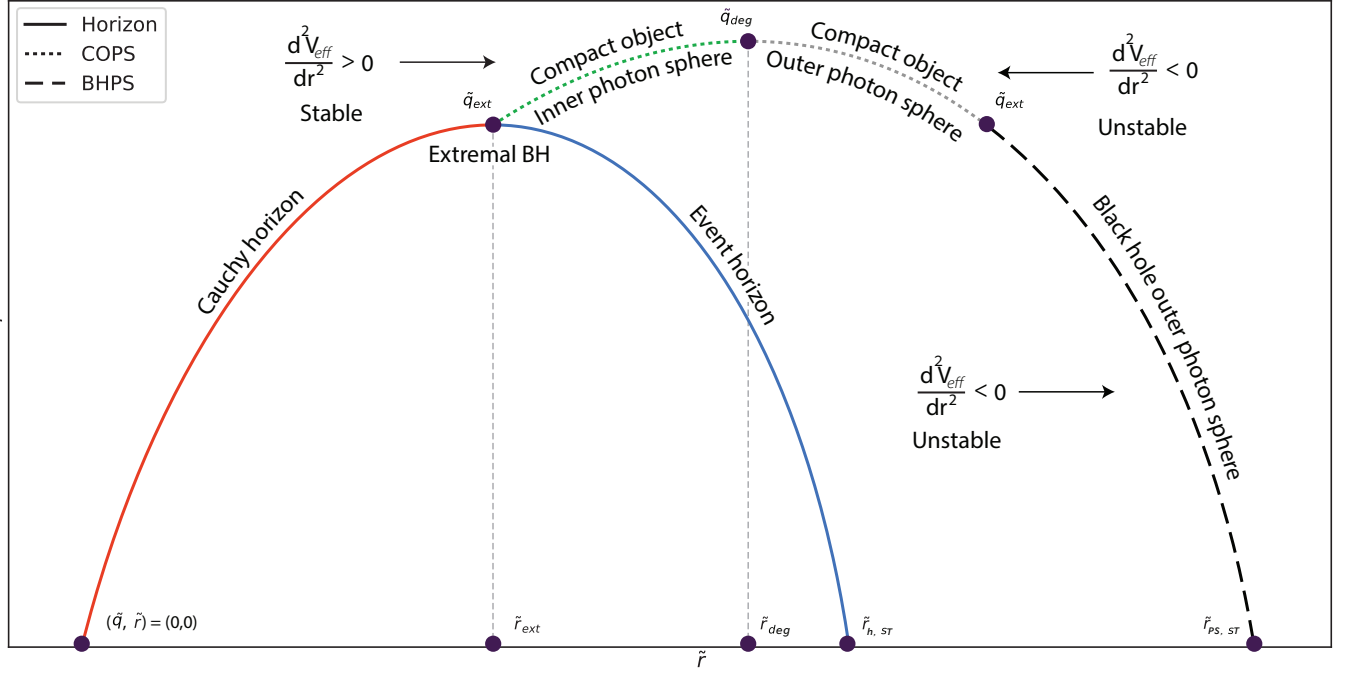


Figure 3: Schematic illustration of the horizons, the BH photon sphere (BHPS), and the compact object photon sphere (COPS), as well as the stability of the photon spheres.

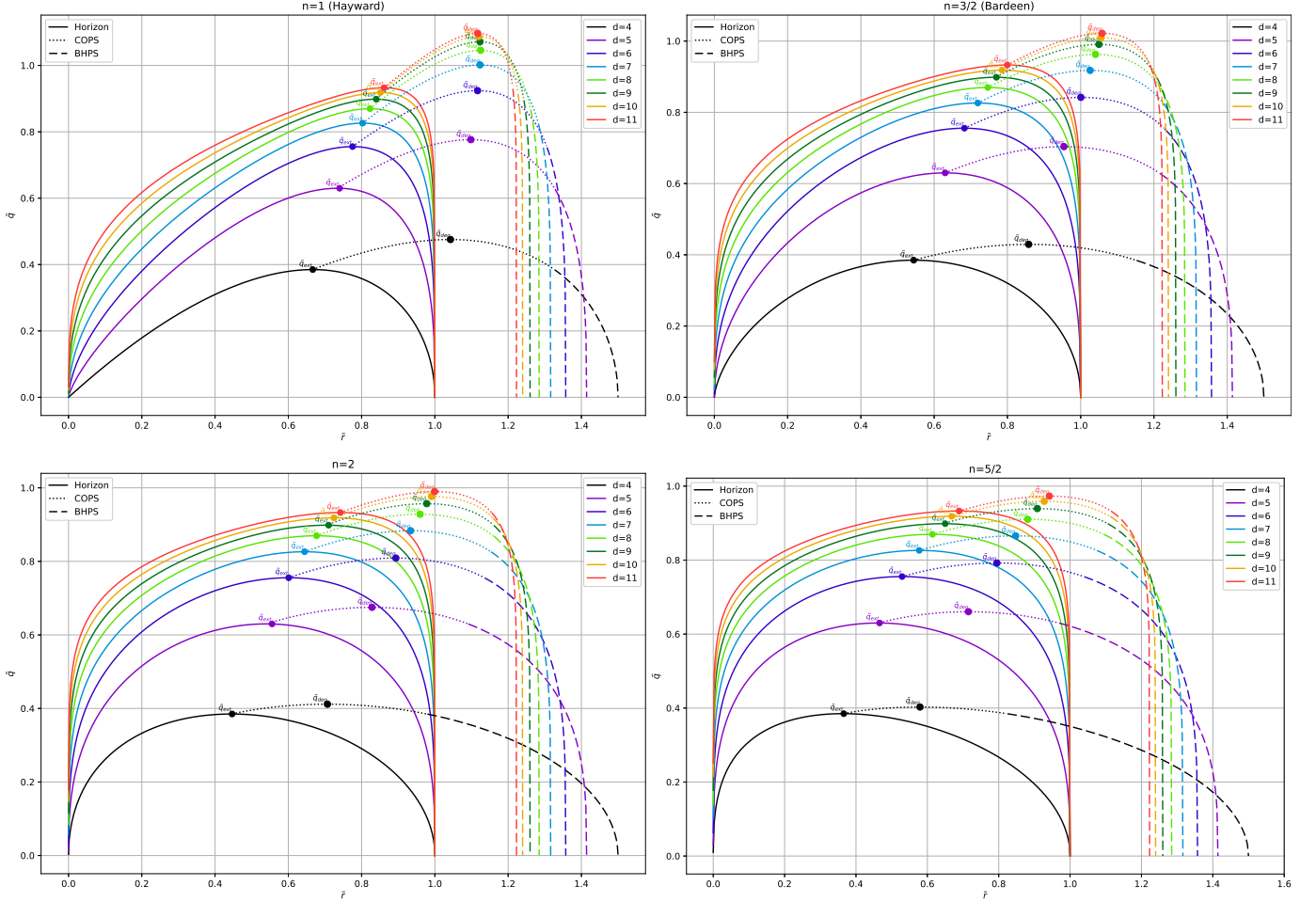


Figure 4: The inner and outer horizons, and photon spheres as a function of \tilde{q} for different dimensions and for $n = 1$ (i.e., Hayward BH), $n = 3/2$ (i.e., Bardeen BH), $n = 2$ and $n = 5/2$ is presented. $\tilde{q} = 0$ represent ST BH.

Table 1: Numerical values for the size of the shadow of the BH using (64). There are no shadows for $\tilde{q} > \tilde{q}_{\text{deg}}$. To observe variations in shadow sizes due to the convergence of radii at lower values of \tilde{q} , appropriate values of \tilde{q} are selected.

$d = 4$								
n	$\tilde{q} = 0.2$	$\tilde{q} = 0.3$	$\tilde{q} = \tilde{q}_{\text{ext}}$	$\tilde{q} = \tilde{q}_{\text{deg}}$	$\tilde{q} = 0.3$	$\tilde{q} = 0.5$	$\tilde{q} = \tilde{q}_{\text{ext}}$	$\tilde{q} = \tilde{q}_{\text{deg}}$
$n = 1$	$\tilde{r} = 2.5659$	$\tilde{r} = 2.5209$	$\tilde{r} = 2.4585$	$\tilde{r} = 2.3292$	$\tilde{r} = 1.9949$	$\tilde{r} = 1.9750$	$\tilde{r} = 1.9455$	$\tilde{r} = 1.8657$
$n = \frac{3}{2}$	$\tilde{r} = 2.5250$	$\tilde{r} = 2.4199$	$\tilde{r} = 2.2620$	$\tilde{r} = 2.1033$	$\tilde{r} = 1.9870$	$\tilde{r} = 1.9351$	$\tilde{r} = 1.8512$	$\tilde{r} = 1.7437$
$n = 2$	$\tilde{r} = 2.4787$	$\tilde{r} = 2.3057$	$\tilde{r} = 2.0344$	$\tilde{r} = 1.8673$	$\tilde{r} = 1.9775$	$\tilde{r} = 1.8864$	$\tilde{r} = 1.7307$	$\tilde{r} = 1.6088$
$n = \frac{5}{2}$	$\tilde{r} = 2.4302$	$\tilde{r} = 2.1881$	$\tilde{r} = 1.8014$	$\tilde{r} = 1.6379$	$\tilde{r} = 1.9672$	$\tilde{r} = 1.8336$	$\tilde{r} = 1.5976$	$\tilde{r} = 1.4703$
$d = 6$								
n	$\tilde{q} = 0.4$	$\tilde{q} = 0.6$	$\tilde{q} = \tilde{q}_{\text{ext}}$	$\tilde{q} = \tilde{q}_{\text{deg}}$	$\tilde{q} = 0.5$	$\tilde{q} = 0.66$	$\tilde{q} = \tilde{q}_{\text{ext}}$	$\tilde{q} = \tilde{q}_{\text{deg}}$
$n = 1$	$\tilde{r} = 1.7501$	$\tilde{r} = 1.7416$	$\tilde{r} = 1.7234$	$\tilde{r} = 1.6654$	$\tilde{r} = 1.6106$	$\tilde{r} = 1.6065$	$\tilde{r} = 1.5943$	$\tilde{r} = 1.5488$
$n = \frac{3}{2}$	$\tilde{r} = 1.7466$	$\tilde{r} = 1.7223$	$\tilde{r} = 1.6662$	$\tilde{r} = 1.5832$	$\tilde{r} = 1.6080$	$\tilde{r} = 1.5957$	$\tilde{r} = 1.5553$	$\tilde{r} = 1.4874$
$n = 2$	$\tilde{r} = 1.7420$	$\tilde{r} = 1.6975$	$\tilde{r} = 1.5880$	$\tilde{r} = 1.4896$	$\tilde{r} = 1.6046$	$\tilde{r} = 1.5812$	$\tilde{r} = 1.4993$	$\tilde{r} = 1.4160$
$n = \frac{5}{2}$	$\tilde{r} = 1.7370$	$\tilde{r} = 1.6696$	$\tilde{r} = 1.4973$	$\tilde{r} = 1.3904$	$\tilde{r} = 1.6006$	$\tilde{r} = 1.5645$	$\tilde{r} = 1.4320$	$\tilde{r} = 1.3390$
$d = 8$								
n	$\tilde{q} = 0.5$	$\tilde{q} = 0.7$	$\tilde{q} = \tilde{q}_{\text{ext}}$	$\tilde{q} = \tilde{q}_{\text{deg}}$	$\tilde{q} = 0.6$	$\tilde{q} = 0.73$	$\tilde{q} = \tilde{q}_{\text{ext}}$	$\tilde{q} = \tilde{q}_{\text{deg}}$
$n = 1$	$\tilde{r} = 1.5197$	$\tilde{r} = 1.5171$	$\tilde{r} = 1.5084$	$\tilde{r} = 1.4709$	$\tilde{r} = 1.4544$	$\tilde{r} = 1.4530$	$\tilde{r} = 1.4465$	$\tilde{r} = 1.4147$
$n = \frac{3}{2}$	$\tilde{r} = 1.5189$	$\tilde{r} = 1.5105$	$\tilde{r} = 1.4799$	$\tilde{r} = 1.4223$	$\tilde{r} = 1.4533$	$\tilde{r} = 1.4486$	$\tilde{r} = 1.4247$	$\tilde{r} = 1.3745$
$n = 2$	$\tilde{r} = 1.5177$	$\tilde{r} = 1.5012$	$\tilde{r} = 1.4372$	$\tilde{r} = 1.3648$	$\tilde{r} = 1.4517$	$\tilde{r} = 1.4422$	$\tilde{r} = 1.3908$	$\tilde{r} = 1.3266$
$n = \frac{5}{2}$	$\tilde{r} = 1.5163$	$\tilde{r} = 1.4903$	$\tilde{r} = 1.3846$	$\tilde{r} = 1.3021$	$\tilde{r} = 1.4499$	$\tilde{r} = 1.4346$	$\tilde{r} = 1.3481$	$\tilde{r} = 1.2737$
$d = 10$								
n	$\tilde{q} = 0.65$	$\tilde{q} = 0.75$	$\tilde{q} = \tilde{q}_{\text{ext}}$	$\tilde{q} = \tilde{q}_{\text{deg}}$	$\tilde{q} = 0.77$	$\tilde{q} = 0.85$	$\tilde{q} = \tilde{q}_{\text{ext}}$	$\tilde{q} = \tilde{q}_{\text{deg}}$
$n = 1$	$\tilde{r} = 1.4053$	$\tilde{r} = 1.4045$	$\tilde{r} = 1.3995$	$\tilde{r} = 1.3720$	$\tilde{r} = 1.3664$	$\tilde{r} = 1.3652$	$\tilde{r} = 1.3624$	$\tilde{r} = 1.3381$
$n = \frac{3}{2}$	$\tilde{r} = 1.4044$	$\tilde{r} = 1.4015$	$\tilde{r} = 1.3822$	$\tilde{r} = 1.3378$	$\tilde{r} = 1.3642$	$\tilde{r} = 1.3596$	$\tilde{r} = 1.3483$	$\tilde{r} = 1.3085$
$n = 2$	$\tilde{r} = 1.4030$	$\tilde{r} = 1.3971$	$\tilde{r} = 1.3545$	$\tilde{r} = 1.2968$	$\tilde{r} = 1.3608$	$\tilde{r} = 1.3510$	$\tilde{r} = 1.3252$	$\tilde{r} = 1.2726$
$n = \frac{5}{2}$	$\tilde{r} = 1.4014$	$\tilde{r} = 1.3917$	$\tilde{r} = 1.3189$	$\tilde{r} = 1.2511$	$\tilde{r} = 1.3567$	$\tilde{r} = 1.3403$	$\tilde{r} = 1.2949$	$\tilde{r} = 1.2325$

As the number of dimensions increases, magnetic charge-dependent shadows also tend to converge. The same is true for the position of horizons, BHPSSs, and COPSSs. As the number of dimensions increases, the differences between the radius of the photon sphere and the radius of the shadow decrease. As these differences become negligible in higher dimensions, studying horizons and photon spheres in detail becomes less important. Consequently, complex mathematical calculations for higher dimensions seem unnecessary.

5 BH Thermodynamics

To study the thermodynamics of the static spherically symmetric BH spacetime (1), it is necessary to find its surface gravity. Since the spacetime is static, the event horizon is also a Killing horizon, which is generated by the Killing vector ξ^μ . Using the metric component (23), the surface gravity is defined as $\kappa = \sqrt{-\xi_{\mu;\nu}\xi^{\mu;\nu}/2}|_{r=r_h}$, which is evaluated at the event horizon, $r = r_h$ and can be simplified to

$$\kappa = \frac{1}{2} \frac{dA_d(r)}{dr} \Big|_{r=r_h} = \left[\frac{1}{2r} \frac{(d-3) - 2m^{\left(\frac{d-2}{2}\right)\left(\frac{3}{n}-2\right)} q^{d-2} r^{-\frac{3(d-2)}{2n}}}{1 + m^{\left(\frac{d-2}{2}\right)\left(\frac{3}{n}-2\right)} q^{d-2} r^{-\frac{3(d-2)}{2n}}} \right]_{r=r_h}. \quad (66)$$

This can be expressed in terms of the dimensionless variables obtained by normalizing m , i.e., the tiled variables in the previous sections, as

$$\bar{\kappa} = \left[\frac{1}{2\tilde{r}} \frac{(d-3) - 2\tilde{q}^{d-2} \tilde{r}^{-\frac{3(d-2)}{2n}}}{1 + \tilde{q}^{d-2} \tilde{r}^{-\frac{3(d-2)}{2n}}} \right]_{\tilde{r}=\tilde{r}_h}. \quad (67)$$

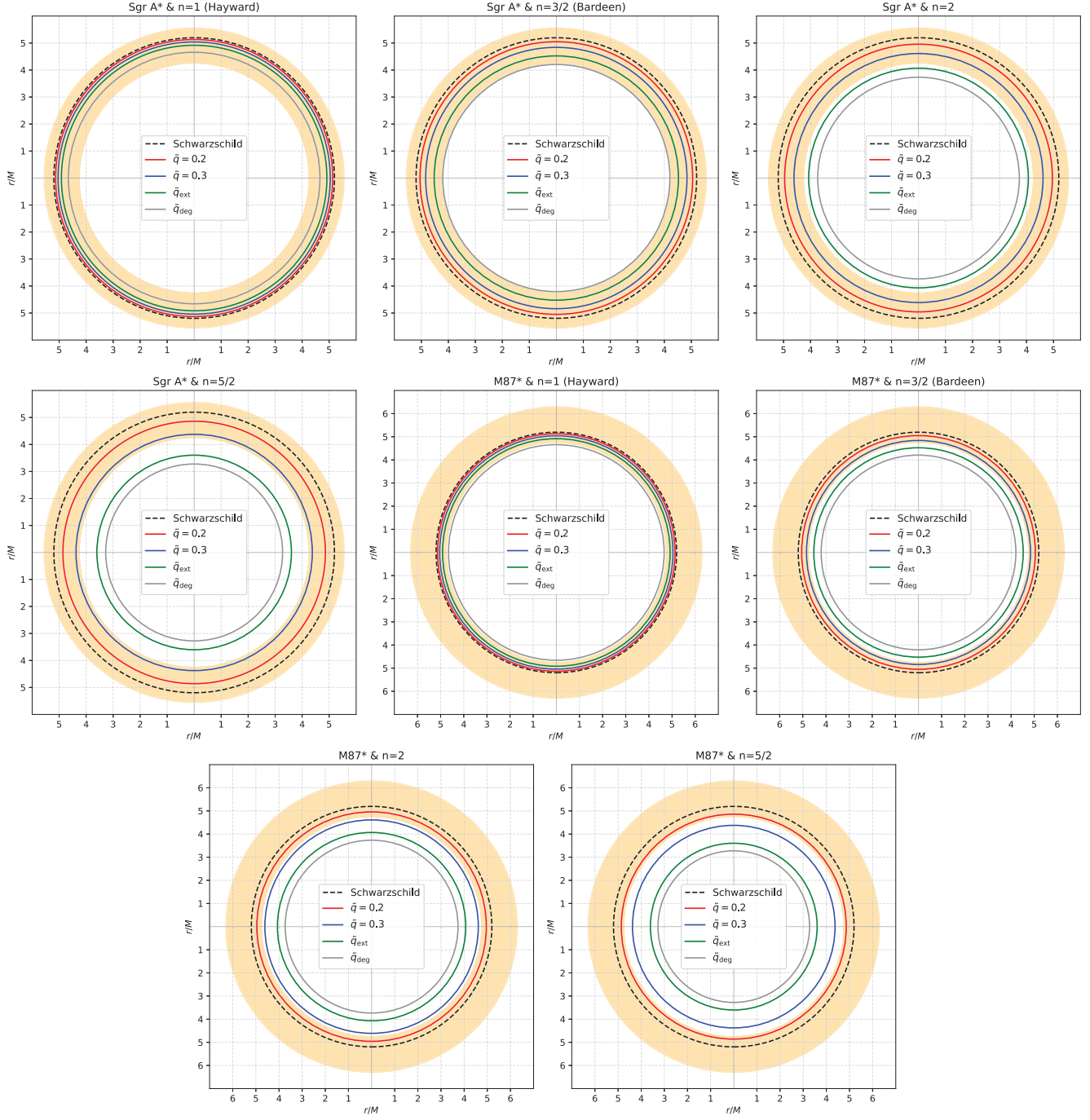


Figure 5: Shadow of the regular 4-dimensional metric (9) compared to the shadow boundaries of $SgrA^*$ and $M87^*$ for various polytropic indices. The dashed line corresponds to the Schwarzschild BH.

where $\bar{\kappa} = m\kappa$. For small values of \tilde{q} , it is clear that the surface gravity tends to that of the ST spacetime, which is $(d-3)/2\tilde{r}_h$. As expected, it can also be seen that in the extremal case, $\tilde{q} = \tilde{q}_{ext}$, the surface gravity becomes zero.

We can plot the Hawking temperature $T = \kappa/2\pi$ as a function of the horizon radius by numerically computing the roots of $A_d(r) = 0$ and then substituting them into the surface gravity (66). See Fig. 6. The temperature starts at zero, corresponding to the extremal horizon, and increases as the horizon radius increases. As expected, the temperature tends to the ST temperature for a sufficiently large horizon radius, corresponding to $m \gg q$.

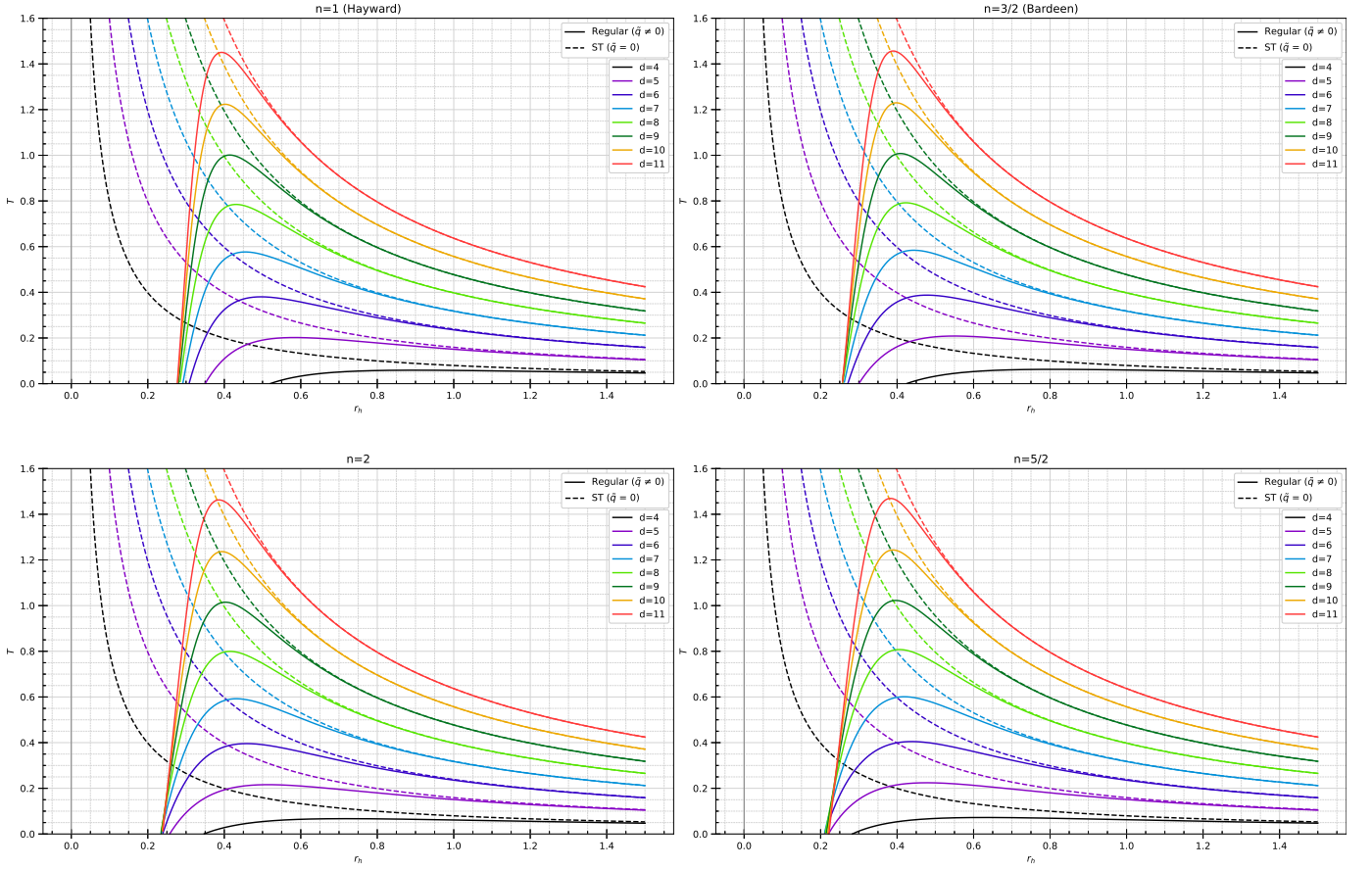


Figure 6: The numerical result of the horizon temperature as a function of the horizon radius for different polytropic index values and dimensions with $q = 0.3$. The solid and dashed lines represent the regular BH (23) and the ST BH, respectively. The horizon temperature begins at zero at the extremal radius. As r_h increases, the temperature decreases for all dimensions.

5.1 Entropy

The thermodynamic properties [26, 27, 50] of a BH, which is described by mass and charge parameters, are defined by

$$T = \frac{\partial M}{\partial S} = \frac{\kappa}{2\pi}, \quad \Phi = \frac{\partial M}{\partial q}, \quad S = \int \frac{1}{T} (dM - \Phi dq) \quad (68)$$

where T is the temperature, Φ is the electric or magnetic potential, S is the Bekenstein-Hawking entropy, and M is the ADM mass introduced in (6). The first law is given by [26, 51]

$$\delta M = T \delta S + \Phi \delta q. \quad (69)$$

Here, δ denotes variations of the BH's parameters. With constant charge, the entropy can then be calculated as

$$S = \int_{r_{\text{ext}}}^{r_h} \frac{1}{T} \left(\frac{\partial M}{\partial r_h} \right)_q dr_h. \quad (70)$$

As shown in Fig. 6, the temperature becomes negative below a minimum horizon radius, which is physically unacceptable. This minimum radius corresponds to the extremal horizon radius r_{ext} , defined as the radius at which the surface gravity (66) vanishes. It is obtained by Eqs.(31) and (32) as

$$r_{\text{ext}} = q_{\text{ext}} \left(\frac{2}{d-3} \right)^{\frac{1}{d-2}} \left(\frac{2}{d-1} \right)^{\frac{(d-1)(2n-3)}{3(d-3)(d-2)}}. \quad (71)$$

Now, we consider the special case of a d -dimensional Bardeen BH ($n = 3/2$), for which the entropy can be derived analytically. Using (23)

$$M_{\text{Bardeen, } d} = \frac{(d-2)\Omega_{d-2}}{16\pi r_h^2} (q^{d-2} + r_h^{d-2})^{\frac{d-1}{d-2}}. \quad (72)$$

whose derivative with respect to the horizon radius is given by

$$\frac{\partial M_{\text{Bardeen, } d}}{\partial r_h} = \frac{(d-2)\Omega_{d-2}}{16\pi r_h^3} (q^{d-2} + r_h^{d-2})^{\frac{1}{d-2}} ((d-3)r_h^{d-2} - 2q^{d-2}). \quad (73)$$

Therefore, using Eqs. (66) and (70), the entropy of a d -dimensional Bardeen BH becomes

$$S_{\text{Bardeen, } d} = \int_{r_{\text{ext}}}^{r_h} \frac{(d-2)\Omega_{d-2}}{4r_h^2} (q^{d-2} + r_h^{d-2})^{\frac{d-1}{d-2}} dr_h, \quad (74)$$

$$\begin{aligned} &= -\frac{(d-2)\Omega_{d-2}}{4r_h q^{d-2}} (q^{d-2} + r_h^{d-2})^{\frac{2d-3}{d-2}} {}_2F_1 \left[1, 2, \frac{d-3}{d-2}, -\frac{r_h^{d-2}}{q^{d-2}} \right] \\ &\quad + \frac{(d-2)\Omega_{d-2}}{4} q^{d-2} \left(\frac{d-1}{d-3} \right)^{\frac{2d-3}{d-2}} \left(\frac{d-3}{2} \right)^{\frac{1}{d-2}} {}_2F_1 \left(1, 2, \frac{d-3}{d-2}, -\frac{2}{d-3} \right), \end{aligned} \quad (75)$$

where ${}_2F_1$ is the hypergeometric function, and r_{ext} is given by (71). An analytical derivation of the Hayward BH ($n = 1$) entropy is also possible in 4 dimensions. A simple calculation using Eqs. (70) and (75) yields¹

$$S_{\text{Hayward, } d=4} = \pi \left(2q^2 \log \left(\frac{r_h^2 - q^2}{2q^2} \right) + \frac{q^4}{q^2 - r_h^2} + r_h^2 \right) - \frac{5\pi q^2}{2}, \quad (76)$$

$$S_{\text{Bardeen, } d=4} = \frac{\pi}{r_h} (r_h^2 - 2q^2) \sqrt{q^2 + r_h^2} + 3\pi q^2 \ln \left(\sqrt{q^2 + r_h^2} + r_h \right) - 3\pi q^2 \ln \left(q(\sqrt{2} + \sqrt{3}) \right). \quad (77)$$

For $q = 0$ the result of (70) reduces to the entropy of the ST, which obeys the area law [23].

$$S_{\text{ST}} = \frac{\Omega_{d-2}}{4} r_h^{d-2}. \quad (78)$$

To determine the entropy for any n , the horizon radius must be known. However, it is not always possible to solve the horizon equation exactly. Therefore, a numerical approach must be used. Entropy (70) is plotted numerically with respect to the horizon radius in Fig. 7. As can be seen, the area law for entropy ($S = \pi r_h^2$) does not hold in regular spacetimes such as (76) and (77) [56, 57]. Moreover, as the polytropic index n increases, the deviation from the area law decreases. Conversely, as the dimension increases, the deviation becomes significant.

5.2 Heat capacity

The goal of this section is to explore the local stability properties of the regular BH (23) by calculating its heat capacity for a constant magnetic charge. The heat capacity, C_q , determines the local thermodynamic stability of the BH. Specifically, a positive heat capacity $C_q > 0$ indicates that the BH is locally stable under thermal fluctuations, and a negative heat capacity $C_q < 0$ implies that the BH is locally unstable. A change in the sign of C_q is significant because it often signals a phase transition, indicating a critical point in the BH's thermodynamic behavior [17, 28, 52, 57, 58]. The heat capacity can be expressed as:

$$C_q = \left(\frac{\partial M}{\partial T} \right)_q = \left(\frac{\partial M}{\partial r_h} \right)_q \left(\frac{\partial r_h}{\partial T} \right)_q. \quad (79)$$

Therefore, the heat capacity can be obtained using Eqs. (29), (6), and (66). Using a numerical approach, the heat capacity can be computed for various values of d and n . The results are plotted in Fig. 8. For d -dimensional Bardeen and 4-dimensional Hayward spacetimes, an analytical approach is feasible. For d -dimensional Bardeen BH

¹The entropy of a 4-dimensional Bardeen spacetime is reported in [17, 52, 53, 54, 55]. However, the authors did not use the lower bound of the integral. Instead, they set the integration constant to zero (i.e., $q = 0$), which is undesirable. Therefore, our results differ from those in the aforementioned references by a constant.

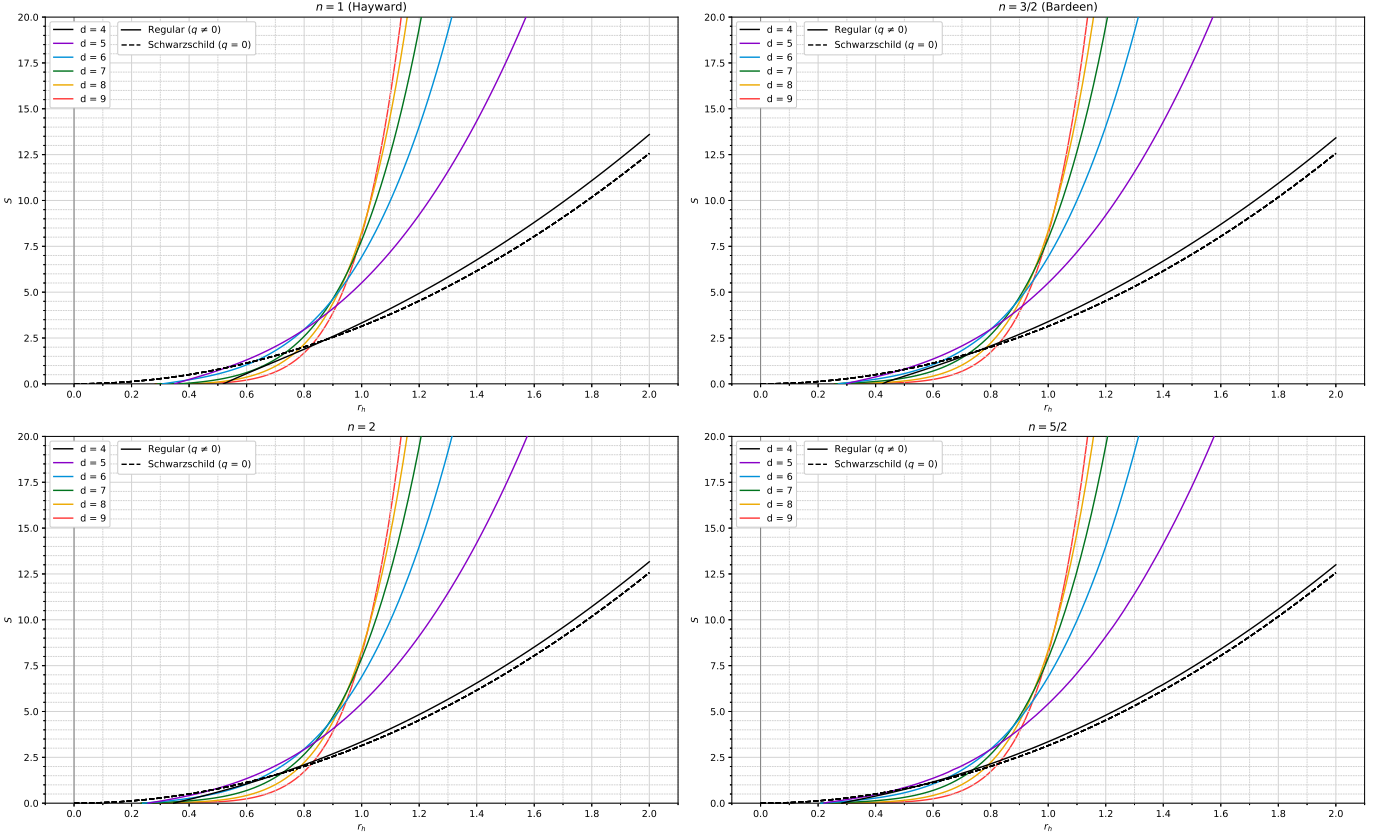


Figure 7: The numerically calculated BH entropy in terms of the outer horizon radius for $q = 0.3$, as well as for different values of the polytropic index and dimensions. The dashed lines represent the Schwarzschild BH entropy in 4 dimensions.

$$C_q|_{\text{Bardeen}, d} = \frac{(d-2)\Omega_{d-2}}{4r_h} \frac{(q^{d-2} + r_h^{d-2})^{\frac{2d-3}{d-2}} ((d-3)r_h^{d-2} - 2q^{d-2})}{(d^2 - 4d + 7) q^{d-2} r_h^{d-2} + 2q^{2(d-2)} - (d-3)r_h^{2(d-2)}}. \quad (80)$$

as well as for 4-dimensional Hayward and Bardeen BHs

$$C_q|_{\text{Hayward}, d=4} = \frac{2\pi r_h^6 (3q^2 - r_h^2)}{(q^2 - r_h^2)^2 (r_h^2 - 9q^2)}, \quad (81)$$

$$C_q|_{\text{Bardeen}, d=4} = \frac{2\pi (q^2 + r_h^2)^{5/2} (r_h^2 - 2q^2)}{r_h (2q^4 + 7q^2 r_h^2 - r_h^4)}, \quad (82)$$

These results are the same as those in [59, 60, 61]. Furthermore, in the limit of $q \rightarrow 0$

$$C_{\text{ST}} = -\frac{(d-2)\Omega_{d-2}}{4} r_h^{d-2}, \quad (83)$$

we recover the heat capacity of the d -dimensional ST BH [62]. The negative value across all radii indicates that the BH is thermodynamically unstable. Unlike the ST BH, the regular BH (23) has a singularity in its heat capacity, which signals a possible phase transition. For the d -dimensional Bardeen BH, this occurs at

$$r_{\text{PT}} = q \left(4(-7 + 4d - d^2 + \sqrt{(d-1)(d((d-7)d+23)-25)} - 7) \right)^{\frac{1}{2-d}}. \quad (84)$$

As Fig. 8 shows, the heat capacity sign is negative and therefore the BH is thermodynamically unstable for horizon radii greater than r_{PT} (indicated by a vertical line), unlike the ST BH. For $r < r_{\text{PT}}$, the BH is stable. The minimum horizon radius is again r_{ext} below which temperature becomes negative and is therefore unacceptable.

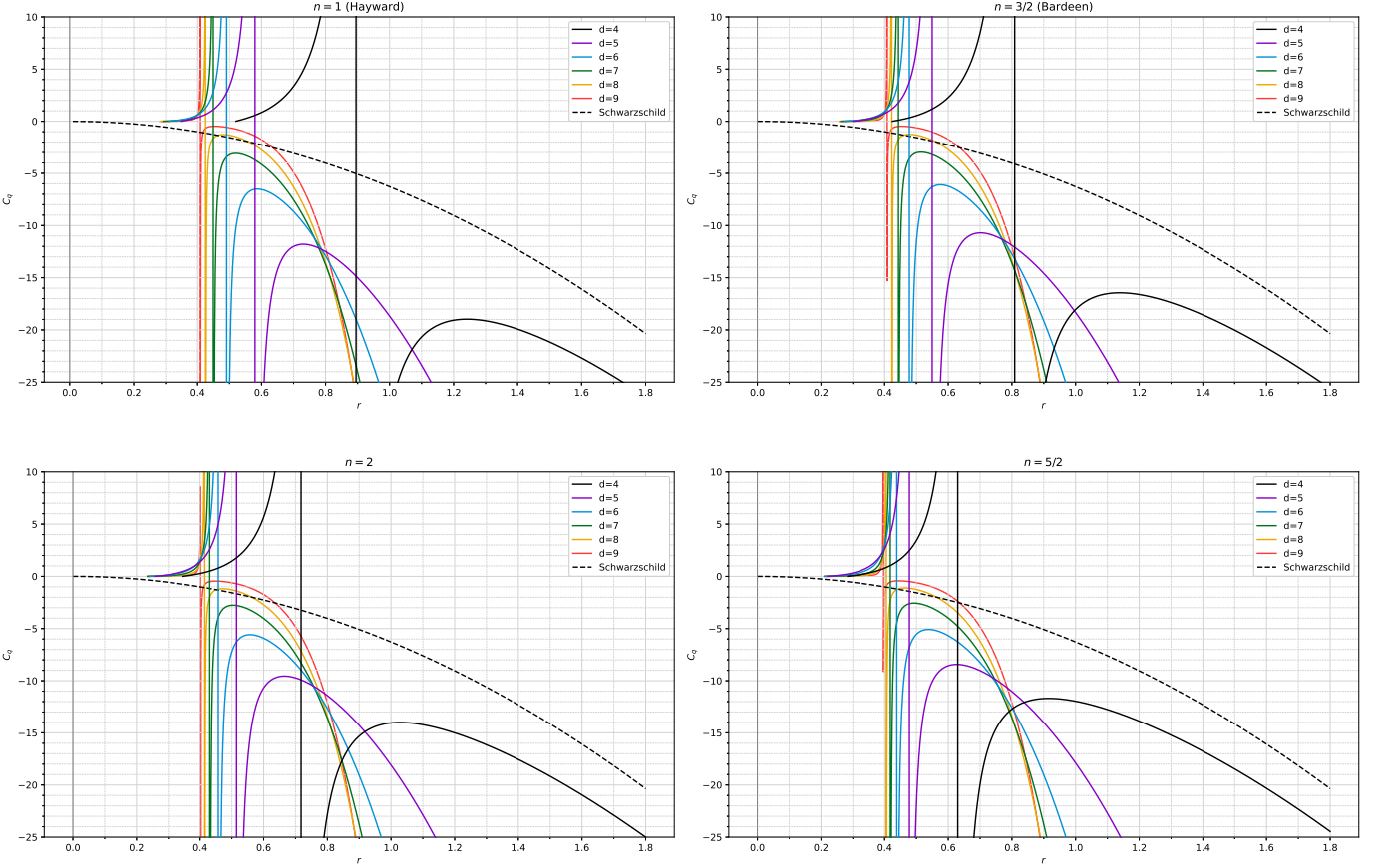


Figure 8: Heat capacity with respect to the horizon radius for different polytropic indices and dimensions, with q set to 0.3. The vertical line indicates the radius at which the heat capacity and its derivative diverge, suggesting a possible phase transition. The dashed line represents a Schwarzschild BH in 4 dimensions.

6 OSD collapse in d dimensions

Considering the spacetime (1), we examine the gravitational collapse of a star in d dimensions according to the OSD model [31, 32]. In the classical OSD scenario, the stellar interior is filled with a homogeneous and isotropic perfect fluid, while the exterior is described by the Schwarzschild solution. The two regions can be smoothly joined without the need for a thin-shell layer.

In our analysis, we embed the star in regular BH spacetime (1) with metric component (23). This generalizes the OSD collapse to d dimensions. The stellar region forms a high-density region relative to its surroundings, leading to gravitational collapse. Although the EMT of the stellar matter is not known a priori, it can be determined by requiring smooth matching of the interior and exterior metrics at the stellar surface. For the interior, we adopt a spatially flat, d -dimensional FLRW metric and choose the time coordinate so that it coincides with the proper time of comoving observers. Meanwhile, the exterior time coordinate is identified with the proper time of freely falling observers.

Based on the assumption we made in section 4, we restrict ourselves to $\theta_i = \pi/2$ (except for θ_{d-2}), and assume that the stellar surface moves radially, equivalent to setting $L = 0$ in Eq. (49). Additionally, we assume that the stellar surface is timelike (i.e., $\epsilon = -1$). Under these conditions, Eq. (50) reduces to

$$E^2 = \dot{r}^2 + A_d(r). \quad (85)$$

If we set r_i as the initial radius of the collapsing star and take it to be sufficiently large, then $E \rightarrow 1$. Thus, it is convenient to write the metric (1) in the Painlevé-Gullstrand (PG) coordinates [63, 64, 65], which describe a freely falling radial observer starting from rest at infinity. The four-velocity of such an observer takes the following form $u^\alpha \partial_\alpha = A_d(r)^{-1/2} \partial_t - \sqrt{1 - A_d(r)} \partial_r$. This gives the observer's proper time τ as $d\tau = dt + A_d(r)^{-1} \sqrt{1 - A_d(r)} dr$.

Substituting this expression for dt into the metric (1) leads directly to its PG representation

$$ds^2 = -d\tau^2 + \left(dr^2 + \sqrt{1 - A_d(r)} d\tau^2 \right) + r^2 d\Omega_{d-2}^2. \quad (86)$$

The interior metric in PG coordinates is also expressed as

$$ds^2 = -d\tau^2 + (dr - rH(\tau)d\tau)^2 + r^2 d\Omega_{d-2}^2, \quad (87)$$

where $r(\tau) = a(\tau)r_c$, $H(\tau) = \dot{r}(\tau)/r(\tau)$, $a(\tau)$ is the scale factor and r_c is the comoving radial coordinate.

The parametric equations on the surface of the star are described by $r = R(\tau)$ and $t = T(\tau)$ where τ is the proper time of observers comoving with the surface [66]. On the surface of the star Σ

$$ds_{\Sigma}^2 = -d\tau^2 + a^2(\tau)R_c d\Omega_{d-2}^2 \quad \text{from inside} \quad (88)$$

$$ds_{\Sigma}^2 = -(A_d(R)\dot{T}^2 - A_d(R)^{-1}\dot{R})d\tau^2 + R^2 d\Omega_{d-2}^2 \quad \text{from outside} \quad (89)$$

According to the Israel junction conditions [67], the induced metric and the extrinsic curvature should be continuous across the boundary of the two geometries to get a smooth transition. The continuity of the induced metric implies $R(\tau) = a(\tau)R_c$ and $A(R)\dot{T}^2 - A(R)^{-1}\dot{R}^2 = 1$. To impose the second junction condition, the extrinsic curvature must be identical on both sides of the stellar surface

$${}^{(\text{in})}K_{\tau}^{\tau} = 0, \quad {}^{(\text{in})}K_{\theta_i}^{\theta_i} = 1/R, \quad (90)$$

$${}^{(\text{out})}K_{\tau}^{\tau} = \dot{\gamma}/\dot{R}, \quad {}^{(\text{out})}K_{\theta_i}^{\theta_i} = \gamma/R, \quad (91)$$

where $\gamma = \sqrt{\dot{R}^2 + A_d(r)}$. To smoothly join two geometries, we require $\gamma = 1$. This yields the evolutionary equation of the stellar surface as

$$\dot{R}(\tau) = -\sqrt{1 - A_d(R)}. \quad (92)$$

The negative sign is chosen due to the contraction of the star. To obtain the Friedmann equation in d dimensions, we must compute the components of the Einstein tensor:

$$G^t_t = -\frac{(d-1)(d-2)}{2} \frac{\dot{a}^2}{a^2} = -8\pi\rho_{\text{star}}, \quad (93)$$

$$G^r_r = G^{\theta_i}_{\theta_i} = -\frac{(d-2)(d-3)}{2} \frac{\dot{a}^2}{a^2} - (d-2) \frac{\ddot{a}}{a} = 8\pi p_{\text{star}}. \quad (94)$$

The first is the Friedmann equation in d dimensions. Substituting $R(\tau) = a(\tau)R_c$ and Eq. (92) into it yields

$$\rho_{\text{star}} = \frac{(d-1)(d-2)}{2} \frac{1 - A_d(R(\tau))}{8\pi R(\tau)^2}. \quad (95)$$

Using Eq. (93) and (94), the continuity equation becomes $\dot{\rho} + (d-1)(\rho + p)\dot{a}/a = 0$. Combining the continuity equation with the density function (95), the stellar pressure can be calculated as

$$p_{\text{star}} = \frac{d-2}{16\pi R(\tau)^2} (R(\tau)A'_d(R(\tau)) + (d-3)(A_d(R(\tau)) - 1)). \quad (96)$$

The isotropic density (95) and pressure (96) provide the total energy density and the isotropic pressure evaluated at the stellar surface. These quantities are a combination of the background contribution from (8) and an additional source associated with the star itself. It should be mentioned that the radial pressure of the exterior metric (3) is equal to the pressure at the surface of the star (96) and as a result the pure radial pressure on the stellar surface is $p_{\text{star}} - p_r|_{r=R} = 0$. Thus, the surface of the star can be specified by null radial pressure and so each particle follows the radial geodesic.

By dividing (95) by (3), using the fact that $p_{\text{star}} = p_r|_{r=R}$ and substituting the resulting radius into (96), straightforward calculations show that the equation of state takes the form

$$p_{\text{star}} = - \left(\frac{16\pi q^{\frac{1}{3}(d-1)(2n)}}{(d-2)(d-1)m^{\frac{2}{3}(d-1)n + \frac{3-4n}{n}}} \right)^{\frac{3(d-2)}{2(d-1)n}} \rho_{\text{star}}^{\frac{3(d-2)}{2(d-1)n} + 1} \quad (97)$$

In 4 dimensions, the equation of state describes a polytropic fluid $p \propto \rho^{1+1/n}$ but for higher dimensions, it describes a generalized polytropic fluid, $p \propto \rho^{1+1/n_{eff}}$, with a dimension-dependent polytropic index $n_{eff} = \frac{2(d-1)}{3(d-2)}$.

Using the energy conditions studied in subsection 3.2 and substituting the metric component (23) into (95) and (8), we find that all energy conditions are satisfied for all radii, except the SEC, which is only satisfied for

$$R_{\text{SEC}} > \left(\frac{(d-3)m^{(d-2)(1-\frac{3}{2n})}}{2q^{d-2}} \right)^{-\frac{2n}{3(d-2)}}, \quad (98)$$

This means that for other radii, the stellar matter contains exotic matter.

6.1 OSD collapse into d -dimensional regular BH

By substituting $A_d(r)$ from (23) into (92) and performing the integration, we obtain the evolution of the stellar surface

$$\begin{aligned} \tau = \frac{2}{d-1} & \left(-\frac{R^{\frac{d-1}{2}}}{m^{\frac{d-3}{2}}} {}_2F_1 \left[\sigma, \sigma; 1-\sigma; -m^{\frac{1}{2}(d-2)(\frac{3}{n}-2)} q^{d-2} R^{-\frac{3(d-2)}{2n}} \right] \right. \\ & \left. + \frac{R_0^{\frac{d-1}{2}}}{m^{\frac{d-3}{2}}} {}_2F_1 \left[\sigma, \sigma; 1-\sigma; -m^{\frac{1}{2}(d-2)(\frac{3}{n}-2)} q^{d-2} R_0^{-\frac{3(d-2)}{2n}} \right] \right), \end{aligned} \quad (99)$$

where ${}_2F_1$ is the hypergeometric function, $\sigma = -\frac{n(d-1)}{3(d-2)}$, and the integration constant R_0 is chosen such that $R = R_0$ at $\tau = 0$. For $n = 1$ and $n = 3/2$ in $d = 4$ we will recover the OSD collapse into Hayward and Bardeen BHs, respectively, as studied in [11]. For $q = 0$, the stellar surface evolution reduces to that of the ST spacetime

$$\tau_{\text{ST}} = \frac{2m^{\frac{3-d}{2}}}{d-1} (R^{\frac{d-1}{2}} - R_0^{\frac{d-1}{2}}), \quad (100)$$

and for $d = 4$, we recover the result of standard OS collapse $\tau_{\text{Sch}} = \frac{2}{3\sqrt{m}} (R^{3/2} - R_0^{3/2})$ [68, 69]. Using the dimensionless parameters, Eq. (99) is plotted in Fig. 9 for various polytropic indices and spacetime dimensions, with the magnetic charge held fixed. As it is evident from Eq. (99), the collapsing stellar surface takes infinite proper time to reach the center (it diverges as $R \rightarrow 0$), so the surface never reaches the center. The duration of the collapse increases with the dimension and polytropic index.

6.1.1 Horizons

Using the metric (87), inside the star, the Hubble parameter can be expressed as $H(\tau) = \dot{R}(\tau)/R(\tau)$ and the radial null trajectories satisfy

$$\frac{dr}{d\tau} = -1 + rH, \quad \text{or} \quad \frac{dr}{d\tau} = 1 + rH. \quad (101)$$

Since $H < 0$, the left expression corresponds to ingoing null geodesics. The right expression represents ingoing null geodesics for $r > -1/H$ and outgoing null geodesics for $r < -1/H$. This means that there are trapped surfaces with radii greater than $-1/H$. Therefore, using Eqs. (92) and (23), the apparent horizon as a function of radius of star can be calculated as

$$r_{\text{AH}} = -\frac{1}{H} = \frac{R^{\frac{d-1}{2}}}{m^{\frac{d-3}{2}}} \left(1 + \frac{m^{\frac{d-2}{2}(\frac{3}{n}-2)} q^{d-2}}{R^{\frac{3(d-2)}{2n}}} \right)^{\frac{n(d-1)}{3(d-2)}}. \quad (102)$$

Eq. (99) together with Eq. (102) describe the evolution of the apparent horizon during the OSD collapse into the d -dimensional regular BH (23). The apparent horizon is plotted as a dotted line in Fig. 9. It forms when the stellar surface crosses the exterior event horizon and vanishes when the surface reaches the exterior Cauchy horizon.

By applying (92), the equation describing the apparent horizon surface can be written as

$$F(r, \tau) = r - \frac{R(\tau)}{\sqrt{1 - A_d(R(\tau))}}. \quad (103)$$

On the horizon $RH/\sqrt{1 - A_d(R)} = -1$, so the normal vector to the apparent horizon is

$$n_a = \partial_a F = - \left(1 + \frac{RA'_d(R)}{2(1 - A_d(R))}, 1, 0, 0 \right). \quad (104)$$

Thus,

$$\begin{aligned} n_a n^a &= - \left(1 + \frac{RA'_d(R)}{2(1 - A_d(R))} \right)^2 + 2 \left(1 + \frac{RA'_d(R)}{2(1 - A_d(R))} \right) \\ &= \frac{4(d-1)q^{d-2}m^{\frac{d-2}{2}(\frac{3}{n}-2)}R^{-\frac{3(d-2)}{2n}} - (d-5)(d-1)}{4 \left(q^{d-2}m^{\frac{1}{2}(d-2)(\frac{3}{n}-2)}R^{-\frac{3(d-2)}{2n}} + 1 \right)^2} \end{aligned} \quad (105)$$

For $d = 4$ and $d = 5$, the above expression is positive. Therefore, the apparent horizon is timelike, but for $d > 5$, the apparent horizon will be null for

$$R_{\text{AH}}^{\text{null}} = \left(\left(\frac{4}{d-5} \right)^{1/3} q^{\frac{d-2}{3}} m^{-\frac{(d-2)(2n-3)}{6n}} \right)^{\frac{2n}{d-2}} \quad (106)$$

and for $R > R_{\text{AH}}^{\text{null}}$ the apparent horizon is spacelike.

To determine the interior event horizon, r_{EH} , we consider the outgoing null geodesics that reach the stellar surface precisely when it intersects the exterior event horizon. As mentioned earlier, outgoing null geodesics satisfy

$$\dot{r}_{\text{EH}} = 1 + r_{\text{EH}} H. \quad (107)$$

Using Eq. (92) and the chain rule $\dot{r}_{\text{EH}} = (dr_{\text{EH}}/dR)\dot{R}$, equation (107) becomes:

$$\frac{dr_{\text{EH}}}{dR} - \frac{r_{\text{EH}}}{R} = - \frac{R^{\frac{d-3}{2}}}{m^{\frac{d-3}{2}}} \left(\frac{q^{d-2} + m^{\frac{d-2}{2}(\frac{3}{n}-2)}}{R^{\frac{3(d-2)}{2n}}} + 1 \right)^{\frac{n(d-1)}{3(d-2)}}. \quad (108)$$

Given the boundary condition $r_{\text{EH}}(r_h) = r_h$, this equation can be solved analytically as

$$\begin{aligned} r_{\text{EH}} &= R - \frac{2R^{\frac{d-1}{2}}}{(d-3)m^{\frac{d-3}{2}}} {}_2F_1 \left[-\frac{n(d-3)}{3(d-2)}, -\frac{n(d-1)}{3(d-2)}; 1 - \frac{n(d-3)}{3(d-2)}; -\frac{m^{\frac{d-2}{2}(\frac{3}{n}-2)}q^{d-2}}{R^{\frac{3(d-2)}{2n}}} \right] \\ &+ \frac{2Rr_h^{\frac{d-3}{2}}}{(d-3)m^{\frac{d-3}{2}}} {}_2F_1 \left[-\frac{n(d-3)}{3(d-2)}, -\frac{n(d-1)}{3(d-2)}; 1 - \frac{n(d-3)}{3(d-2)}; -\frac{m^{\frac{d-2}{2}(\frac{3}{n}-2)}q^{d-2}}{r_h^{\frac{3(d-2)}{2n}}} \right]. \end{aligned} \quad (109)$$

Eqs. (99) and (109) describe the evolution of the event horizon as a function of proper time. See Fig. 9. As the number of dimensions increases, so does the initial radius of the event horizon. In Fig. 9, the value of the parameter $\tilde{q} = 0.3$ is fixed for all plots. With increasing dimensionality, the resulting event horizon approaches that of the Schwarzschild BH, a consequence of the fixed choice of q (see Fig. 4). For the ST BH limit ($q = 0$), Eq. (109) reduces to

$$r_{\text{EH, ST}} = \frac{R}{3-d} \left(\frac{2R^{\frac{d-3}{2}}}{m^{\frac{d-3}{2}}} - d + 1 \right), \quad (110)$$

and for Schwarzschild BH, it becomes $r_{\text{EH, Sch}} = 3R - \frac{2R^{3/2}}{\sqrt{m}}$. An important point concerns the choice of the initial radius R_0 . In addition to the condition $\tilde{R} = \tilde{R}_0$ at $\tilde{\tau} = 0$, the initial radius must be selected such that the event horizon radius remains positive at $\tilde{\tau} = 0$. For collapse to a Schwarzschild BH, the horizon radius vanishes at $\tilde{R} = 9/4$ and becomes positive for $\tilde{R}_0 > 9/4$. This sets a lower bound on the admissible initial radius of the star. Otherwise, the event horizon would form before beginning the OSD collapse, which is unphysical¹. Since the Schwarzschild BH naturally has the largest R_0 limit, we chose $\tilde{R}_0 = 2.5$ in Fig. 9 to satisfy this condition.

¹A straightforward calculation shows that the minimum initial radius R_0 required for physical BH formation with spatially flat interior geometry is determined by

$$1 = \int_{R_+}^{R_{0,\text{min}}} \frac{dR}{R\sqrt{1-f(R)}}. \quad (111)$$

where $g_{tt} = g^{rr} = f(R)$. This condition arises by demanding that the interior event horizon $r_{\text{EH}}(R)$ (here, given by Eq. (108), begins growing from zero radius at the onset of collapse. The above relation applies universally to any static, spherically symmetric exterior geometry characterized by the metric function $f(R)$. For further details and the extension to the spatially closed case see [70].

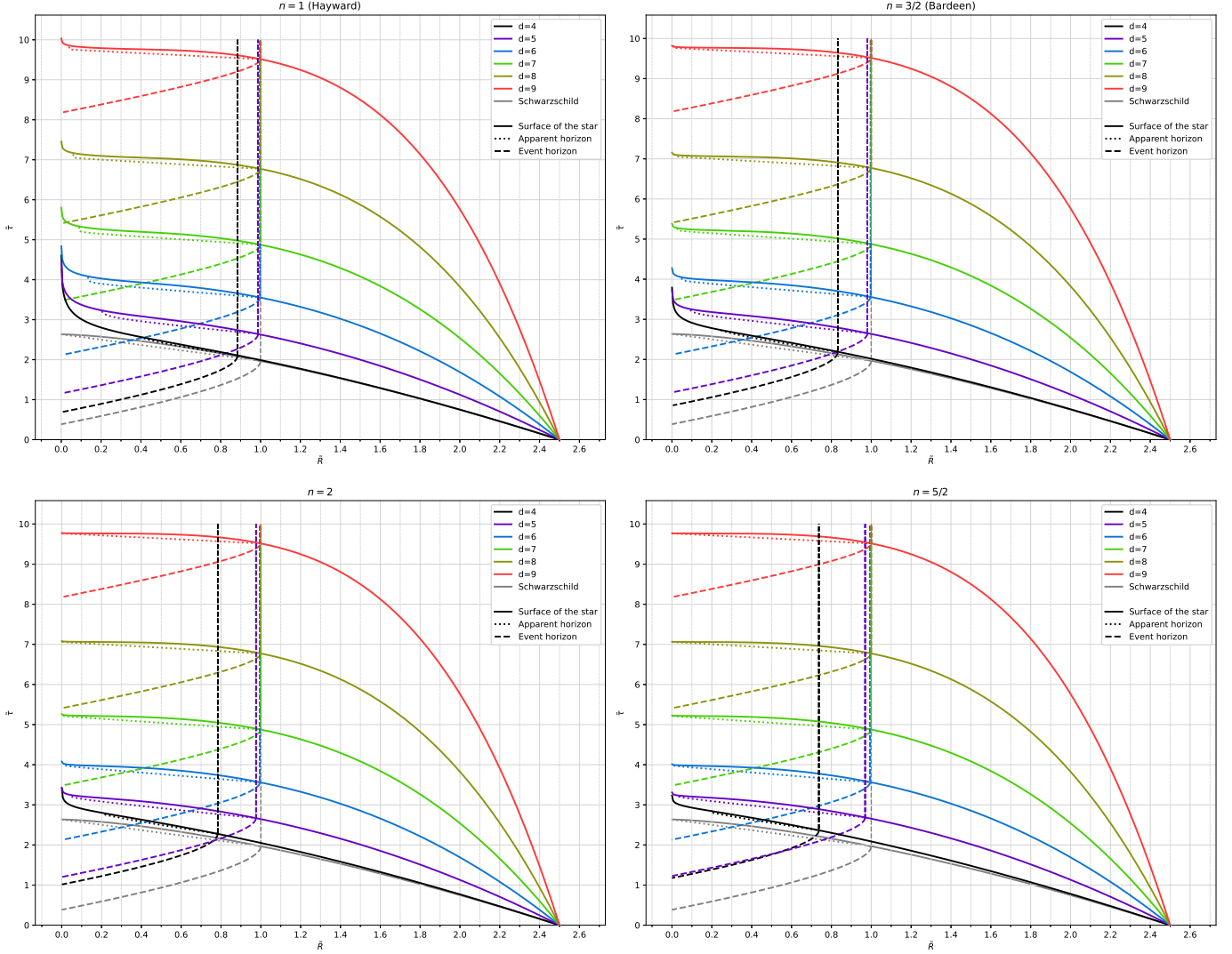


Figure 9: The evolution of the star surface and horizons in OSD collapsing scenario into d -dimensional regular BH (23) for different polytropic indices and dimensions and with the fixed values of $\tilde{q} = 0.3$ and $R_0 = 2.5$. The quantities are normalized to m , which are denoted by tildes. The solid, dotted, and dashed curves represent the surface of the star, the apparent horizon, and the event horizon, respectively. The Schwarzschild case is plotted as a grey line.

7 Conclusion

This paper has focused on the class of 4-dimensional regular BHs with a de Sitter core, which was recently shown to be generated by the collapse of a polytropic star [11]. This class of BHs contains the well-known Bardeen and Hayward regular BHs. We extended this class to the d -dimensional case and considered nonlinear electrodynamics as the source of Einstein's equations. The presence of magnetic charge in the source results in a regular center, whereas its absence results in an ST BH. Our class reduces to d -dimensional Bardeen and Hayward BHs when special values are chosen for the polytropic index.

We have analyzed the horizons, energy conditions, extremal conditions, photon spheres, and shadows of the aforementioned class of BHs. We have demonstrated that the SEC is violated at certain radii and, depending on the polytropic index value, the DEC may also be violated for specific dimensions and radii. Our findings show that, as the number of dimensions increases, the differences in the radii of horizons, photon spheres, and shadows decrease. Photon spheres and shadows persist only up to a limit of magnetic charge which we call q_{deg} . Beyond this limit, the photon spheres and shadow vanish, resulting in a horizonless compact object. Additionally, the extremality condition is independent of the polytropic index. Therefore, it is the same for both Bardeen and Hayward BHs, as well as for other regular BHs belonging to the mentioned class of BHs in 4 dimensions.

We have studied the thermodynamics of our proposed class of d -dimensional regular BHs using the standard definitions of surface gravity, temperature, entropy, and heat capacity. Unlike the ST BH, zero temperature occurs at a minimal horizon radius, i.e, the extremal horizon, r_{ext} . Horizon radii below this value are considered unphysical because they correspond to negative temperature. As the horizon radius increases from r_{ext} , the temperature rises from zero to a maximum, after which it decreases for larger horizon radii.

We have also examined the heat capacity and thermodynamic stability of the aforementioned BH model. Unlike an ST BH, which is always unstable, our proposed d -dimensional regular BHs can be thermodynamically stable for certain horizon radii. They also exhibit possible phase transitions for every dimension and polytropic index.

Furthermore, we have generalized the OSD collapse to d dimensions and replaced the Schwarzschild exterior with a d -dimensional regular BH solution. We have analyzed the evolution of the stellar surface, as well as the apparent and event horizons. As the number of dimensions increases, we have found that the formation of a BH takes a longer proper time. Increasing the polytropic index slightly increases the proper time for collapse as well.

A Analytic solutions

This appendix explores analytical solutions to the event horizon equation (28). For spacetime dimensions $d > 4$, an exact analytical solution is generally unattainable. This is because the horizon equation (28) becomes a quintic equation, which lacks a solution in closed form without introducing simplifying assumptions. However, exact solutions can be obtained for odd dimensions up to $d = 9$. We introduce the scaled parameters $\tilde{r} = r/m$ and $\tilde{q} = q/m$.

A.1 Horizons in 5 dimensions

At $d = 5$, Eq. (28) becomes quadratic and can be easily solved as

$$\tilde{r}_{\pm}^{(5)} = \left(\frac{1}{2} \left(1 \pm \sqrt{1 - 4\tilde{q}^3} \right) \right)^{\frac{4n}{9}}, \quad (\text{A.1})$$

where \tilde{r}_+ is the outer (event) horizon, and \tilde{r}_- is the inner (Cauchy) horizon.

A.2 Horizons in 7 dimensions

At $d = 7$, Eq. (28) becomes a cubic equation with the following form:

$$\tilde{R}^2 - \tilde{q}^5 \tilde{R}^3 - 1 = 0, \quad (\text{A.2})$$

To solve this equation, we convert it into a depressed cubic equation by introducing a new variable x defined as

$$x = \tilde{R} - \frac{1}{3\tilde{q}^5}. \quad (\text{A.3})$$

To solve the horizon equation (28) using this substitution, we must solve the resulting depressed cubic equation for x .

$$x^3 + px + s = 0, \quad (\text{A.4})$$

where

$$p = -\frac{1}{3\tilde{q}^{10}}, \quad s = \frac{1}{\tilde{q}^5} - \frac{2}{27\tilde{q}^{15}}, \quad (\text{A.5})$$

The solution to this equation is

$$x_k = 2\sqrt{\frac{-p}{3}} \cos \left[\frac{1}{3} \arccos \left(\frac{3s}{2p} \sqrt{\frac{-3}{p}} \right) - \frac{2\pi k}{3} \right], \quad (\text{A.6})$$

where $k = 0, 1, 2$. The discriminant is always positive, which guarantees the existence of three distinct real roots. Among these three real roots, two are positive and correspond to the inner and outer horizons. The final form of the solution is given by

$$\tilde{r} = \tilde{q}^{2n} \left(\frac{1}{3} + \frac{2}{3} \cos \left(\frac{2\pi k}{3} - \frac{1}{3} \cos^{-1} \left(\frac{1}{2} (2 - 27\tilde{q}^{10}) \right) \right) \right)^{-\frac{2n}{5}}. \quad (\text{A.7})$$

A.3 Horizons in 9 dimensions

For $d = 9$, Eq.(28) becomes a quartic

$$\tilde{q}^7 \tilde{R}^4 - \tilde{R}^3 - 1 = 0, \quad (\text{A.8})$$

where $\tilde{R} = \tilde{r}^{-\frac{21}{8n}}$. Expressing the quartic equation in its depressed form yields the coefficients of the first and the second degrees in the associated depressed quartics are

$$p = -\frac{3}{8\tilde{q}^{14}}, \quad q = \frac{1}{8\tilde{q}^{21}}, \quad (\text{A.9})$$

Substituting back for \tilde{r} , the solutions are

$$\tilde{r}_{1,2} = \left(\frac{1}{4\tilde{q}^7} - S \pm \frac{1}{4} \sqrt{-\frac{1}{2\tilde{q}^{21}S} + \frac{3}{\tilde{q}^{14}} - 16S^2} \right)^{-\frac{8n}{21}}, \quad (\text{A.10})$$

$$\tilde{r}_{3,4} = \left(\frac{1}{4\tilde{q}^7} + S \pm \frac{1}{4} \sqrt{-\frac{1}{2\tilde{q}^{21}S} + \frac{3}{\tilde{q}^{14}} - 16S^2} \right)^{-\frac{8n}{21}}, \quad (\text{A.11})$$

(A.12)

where

$$S = \frac{1}{4} \sqrt{\frac{4Q}{3\tilde{q}^7} - \frac{16}{Q} + \frac{1}{\tilde{q}^{14}}}, \quad Q = \left(\frac{3}{2} \sqrt{192\tilde{q}^{21} + 81} - \frac{27}{2} \right)^{1/3}. \quad (\text{A.13})$$

To determine the real roots among the four roots, one should calculate the discriminant. The discriminant is $\Delta = -(256\tilde{q}^{21} + 27) < 0$ which indicates that the quartic equation has two real positive roots and two complex conjugate roots. The complex roots are physically irrelevant. Therefore, among the solutions in (A.10) and (A.11), two are real and positive, corresponding to the inner and outer horizons.

References

- [1] V.P. Frolov, G.A. Vilkovisky, in Proceedings of the Second Marcel Grossmann Meeting on General Relativity, Trieste, Italy, 5–11 July (1979); V.P. Frolov, G.A. Vilkovisky, Phys. Lett. B, **106**, 307–313 (1981).
- [2] R. Penrose, Riv. Nuovo, Cim. **1** 252–276 (1969); ibid., Gen. Rel. Grav. **34**, 1141 (2002).
- [3] V. Mukhanov, S. Winitzki, *"Introduction to quantum effects in gravity"*, Cambridge University Press, (2007).
- [4] M. Markov, JETP Letters **36**, 265 (1982); M. Markov, Ann. Phys. **155**, 333 (1984); J. Polchinski, Nucl.Phys. B **325**, 619 (1989).
- [5] V. P. Frolov, Phys. Rev. D. **94**, 104056 (2016).
- [6] A.D. Sakharov, Sov. Phys. JETP **22** 241 (1966).
- [7] E.B. Gliner, Sov. Phys. JETP **22** 378 (1966).
- [8] J.M. Bardeen, in Proceedings of the International Conference GR5, Tbilisi, U.S.S.R. (1968).
- [9] E. Ayón-Beato, A. García, Gen. Rel. Grav. **31** 629 (2003); N. Breton, Phys. Rev. D **67**, 124004 (2003).
- [10] S. A. Hayward, Phys. Rev. Lett. **96**, 031103 (2006).
- [11] F. Shojai, A. Sadeghi, and R. Hassannejad, Class. Quantum Grav. **39**, 8, 085003 (2022).
- [12] A. Strominger and C. Vafa, Phys. Lett. B 379, 99 (1996).
- [13] O. Aharony, S. S. Gubser, J. M. Maldacena, H. Ooguri, and Y. Oz, Phys. Rep. 323, 183 (2000).
- [14] F. R. Tangherlini, Nuovo Cim. **27**, 636-651 (1963).

[15] R. C. Myers and M. J. Perry, Ann. Phys. **172**, 304 (1986).

[16] R. Emparan and H. S. Reall, Living Rev. Rel. **11**, 6 (2008).

[17] M. S. Ali and S. G. Ghosh, Phys. Rev. D **98**, 8, 084025 (2018).

[18] K. Akiyama *et al.* [Event Horizon Telescope], Astrophys. J. Lett. **875**, L1 (2019).

[19] K. Akiyama *et al.* [Event Horizon Telescope], Astrophys. J. Lett. **930**, 2, L12 (2022).

[20] V. Cardoso and P. Pani, Living Rev. Rel. **22**, 1, 4 (2019).

[21] R. Shaikh, Mon. Not. Roy. Astron. Soc. **523**, 1, 375-384 (2023).

[22] A. B. Abdikamalov, A. A. Abdujabbarov, D. Ayzenberg, D. Malafarina, C. Bambi, and B. Ahmedov, Phys. Rev. D **100**, 2, 024014 (2019).

[23] B. P. Singh, and S. G. Ghosh, Ann. Phys. **395**, 127-137 (2018).

[24] S. Roy, S. Chatterjee, and R. Koley, Eur. Phys. J. C **84**, 1, 47 (2024).

[25] U. Papnoi, F. Atamurotov, S. G. Ghosh, and B. Ahmedov, Phys. Rev. D **90**, 2, 024073 (2014).

[26] J. M. Bardeen, B. Carter, and S. W. Hawking, Commun. Math. Phys. **31**, 161-170 (1973).

[27] S. W. Hawking, Commun. Math. Phys. **43**, 199-220 (1975).

[28] A. Bonanno and M. Reuter, Phys. Rev. D **62**, 043008 (2000).

[29] P. Hut, Mon. Not. R. astr. Soc. 180, 379 - 389 (1977).

[30] Diego Pavón, Phys. Rev. D **43**, 2495 - 2497 (1991).

[31] J. R. Oppenheimer and H. Snyder, Phys. Rev. **56**, 455-459 (1939).

[32] B. Datt, Z. Phys. **108**, 5, 314-321 (1938).

[33] Y. Liu, D. Malafarina, L. Modesto and C. Bambi, Phys. Rev. D **90**, 4, 044040 (2014).

[34] Y. Liu, D. Malafarina, L. Modesto and C. Bambi, Phys. Rev. D **88**, 044009 (2013).

[35] Y. Zhang, Y. Zhu, L. Modesto and C. Bambi, Eur. Phys. J. C **75**, 2, 96 (2015).

[36] E. Ayon-Beato and A. Garcia, Phys. Lett. B **493**, 149-152 (2000).

[37] R. C. Myers and M. J. Perry, Ann. Phys. (N.Y.) **172**, 304 (1986).

[38] X. Dianyan, Classical Quantum Gravity **5**, 871 (1988).

[39] Z. Y. Tang, B. Wang and E. Papantonopoulos, Eur. Phys. J. C **81**, 4, 346 (2021).

[40] R. Yin, J. Liang and B. Mu, Phys. Dark Univ. **32**, 100831 (2021).

[41] M. E. Rodrigues and M. V. de Sousa Silva, JCAP **06**, 025 (2018).

[42] D. Malafarina and B. Toshmatov, Phys. Rev. D **105**, 12, L121502 (2022).

[43] D. Malafarina, Malafarina, D. "Semi-classical Dust Collapse and Regular Black Holes", Springer Series in Astrophysics and Cosmology. Springer, Singapore. (2023).

[44] G. Guo, Y. Lu, P. Wang, H. Wu and H. Yang, Phys. Rev. D **107**, 12, 124037 (2023).

[45] J. L. Synge, Mon. Not. Roy. Astron. Soc. **131**, , 3, 463-466 (1966).

[46] V. Perlick and O. Y. Tsupko, Phys. Rept. **947**, 1-39 (2022).

[47] U. Papnoi, F. Atamurotov, S. G. Ghosh and B. Ahmedov, Phys. Rev. D **90**, no.2, 024073 (2014).

[48] C. Bambi, K. Freese, S. Vagnozzi and L. Visinelli, Phys. Rev. D **100**, 4, 044057 (2019).

[49] S. Vagnozzi, R. Roy, Y. D. Tsai, L. Visinelli, M. Afrin, A. Allahyari, P. Bambhaniya, D. Dey, S. G. Ghosh and P. S. Joshi, *et al.* Class. Quant. Grav. **40**, 16, 165007 (2023).

[50] J. Bekenstein, Scholarpedia **3**, 10, 7375 (2008).

[51] L. Smarr, Phys. Rev. Lett. **30**, 71-73 (1973).

[52] J. Man and H. Cheng, [arXiv:1312.6566 [hep-th]].

[53] D. V. Singh and S. Siwach, [arXiv:1909.11529 [hep-th]].

[54] J. Sadeghi, S. Noori Gashti, M. R. Alipour and M. A. S. Afshar, Annals Phys. **455**, 169391 (2023).

[55] M. Sharif and W. Javed, J. Korean Phys. Soc. **57**, 217-222 (2010).

[56] R.M. Wald, Phys. Rev. D **43** R3427 (1993).

[57] D. V. Singh, S. G. Ghosh and S. D. Maharaj, Nucl. Phys. B **981**, 115854 (2022).

[58] P. Chaturvedi, N. K. Singh and D. V. Singh, Int. J. Mod. Phys. D **26**, 08, 1750082 (2017).

[59] J. Man and H. Cheng, Gen. Rel. Grav. **46**, 1660 (2014).

[60] M. Akbar, N. Salem, and S. A. Hussein, Chin. Phys. Lett. **29**, 070401 (2012).

[61] Y. S. Myung, Y. W. Kim and Y. J. Park, Gen. Rel. Grav. **41**, 1051-1067 (2009).

[62] S. G. Ghosh, U. Papnoi and S. D. Maharaj, Phys. Rev. D **90**, 4, 044068 (2014).

[63] P. Painlevé, C. R. Acad. Sci. **173**, 677–680 (1921).

[64] A. Gullstrand, Arkiv för Matematik, Astronomi och Fysik. **16** (8): 1–15 (1922).

[65] K. Martel and E. Poisson, Am. J. Phys. **69**, 476-480 (2001).

[66] E. Poisson, “A Relativist’s Toolkit: The Mathematics of Black-Hole Mechanics,” Cambridge University Press, (2009).

[67] W. Israel, *Nuovo Cimento*, **44** 4349 (1966).

[68] M. Blau, "Lecture note on general Relativity", <http://www.blau.itp.unibe.ch/newlecturesGR.pdf> (2020).

[69] L. Rezzolla, "An Introduction to Gravitational Collapse to Black Holes", Lectures given at the Villa Mondragone International School of Gravitation and Cosmology, Frascati (Rome), Italy, Sept. 7th – 10th, (2004).

[70] A. Sadeghi, "Black hole mimickers", Ph.D. thesis, University of Tehran, (2025); H. Khodabakhshi, H. Lu and F. Shojai, Phys. Rev. D **112**, no.12, 124057 (2025).